creative commons
COMMONS DEED

저작자표시-비영리-변경금지 2.0 대한민국

이용자는 아래의 조건을 따르는 경우에 한하여 자유롭게

- 이 저작물을 복제, 배포, 전송, 전시, 공연 및 방송할 수 있습니다.

다음과 같은 조건을 따라야 합니다:

저작자표시. 귀하는 원저작자를 표시하여야 합니다.

비영리. 귀하는 이 저작물을 영리 목적으로 이용할 수 없습니다.

변경금지. 귀하는 이 저작물을 개작, 변형 또는 가공할 수 없습니다.

- 귀하는, 이 저작물의 재이용이나 배포의 경우, 이 저작물에 적용된 이용허락조건을 명확하게 나타내어야 합니다.
- 저작권자로부터 별도의 허가를 받으면 이러한 조건들은 적용되지 않습니다.

저작권법에 따른 이용자의 권리는 위의 내용에 의하여 영향을 받지 않습니다.

이것은 이용허락규약(Legal Code)을 이해하기 쉽게 요약한 것입니다.

Disclaimer

dCollection

ULSAN NATIONAL INSTITUTE OF SCIENCE AND TECHNOLOGY

Master's Thesis

Combined MoOx buffer layer with metal oxide nanoparticle for improved stability and performance of semi-transparent perovskite solar cell

SangGeun Ji

Department of Energy Engineering

(Energy Engineering)

Graduate School of UNIST

2019

ULSAN NATIONAL INSTITUTE OF
SCIENCE AND TECHNOLOGY

Combined MoOx buffer layer with metal oxide nanoparticle for improved stability and performance of semi-transparent perovskite solar cell

SangGeun Ji

Department of Energy Engineering
(Energy Engineering)

Graduate School of UNIST

ULSAN NATIONAL INSTITUTE OF
SCIENCE AND TECHNOLOGY

Combined MoOx buffer layer with metal oxide nanoparticle for improved stability and performance of semi-transparent perovskite solar cell

A thesis/dissertation
submitted to the Graduate School of UNIST
in partial fulfillment of the
requirements for the degree of
Master of Science

SangGeun Ji

07. 05. 2019
Approved by

_____

Advisor
Sang Il Seok

ULSAN NATIONAL INSTITUTE OF SCIENCE AND TECHNOLOGY

Combined MoOx buffer layer with metal oxide nanoparticle for improved stability and performance of semi-transparent perovskite solar cell

SangGeun Ji

This certifies that the thesis of SangGeun Ji is approved.

07/05/2019

signature

_____

Advisor: Sang Il Seok

signature

_____

Jin Young Kim

signature

_____

Kwanyong Seo

ULSAN NATIONAL INSTITUTE OF SCIENCE AND TECHNOLOGY

Abstract

For the alternative energy of environmental issues such as global warming, solar energy has been researched as an example of the green energies. For the operation of solar cell, it required basic process of generating electron/hole pairs by absorbing light, separating charge carriers, and extracting those carriers to external circuit. And for these requirements, semiconducting materials have been used because of the high ability of absorbing the sunlight and generating charge carriers. And as the research progressed, perovskite materials were spotlighted as a semiconducting material because of their cheap costs and simple processes for fabrication. Perovskite solar cell's efficiency had been increased from below 5% in 2009 to 24.2% in 2019. In addition, from a structural point of view, perovskite thin film was adapted to the multijunction solar cells to exceed the theoretical maximum efficiency (Shockley-Queisser limit). Initially, in multijunction solar cell, perovskite solar cell was normally combined with silicon semiconductor with different absorption band width. For the multijunction solar cell, perovskite solar cell should be semi-transparent to transmit solar light to the bottom silicon subcell. And for coating the transparent electrode, magnetron sputtering process was commonly used, while opaque electrodes were coated by thermal evaporation. But during the magnetron sputtering process, the plasma from sputtering environment induced a damage to the organic charge transfer layer. In the ITO directly sputtered solar cell, the organic layer had been degraded with decreased fill factor and efficiency. For this reason, it was necessary to coat additional buffer layer to block the plasma damage while sputtering. Molybdenum oxide (MoO_x) has been mostly used material as the buffer layer by thermal evaporation on hole transfer layer. Obviously, the semi-transparent perovskite cell with MoO_x buffer layer showed higher efficiency than pristine device. But in the stability issues, MoO_x showed hygroscopic property that could easily pass the moisture to the under layers. For example, MoO_x contained opaque device with Au/Ag electrode greatly degraded its efficiency just after few hours. And we found that semi-transparent perovskite cell with MoO_x layer also showed bad stability in thermal environment condition. We tried to solve this stability issue by coating additional metal oxide nanoparticles as a buffer layer before MoO_x coating. With mixed buffer layer of nanoparticles and MoO_x, the semi-transparent perovskite solar cell showed enhanced stability both in ambient and thermal environment conditions. Furthermore, the performances of semi-transparent perovskite solar cell were also increased.

ULSAN NATIONAL INSTITUTE OF
SCIENCE AND TECHNOLOGY

ULSAN NATIONAL INSTITUTE OF SCIENCE AND TECHNOLOGY

Contents

Abstract ---------- 5

List of Figures ---------- 8

List of Tables ---------- 11

I. Introduction

1.1 History of Perovskite Solar Cell ---------- 12

1.2 Perovskite material tuning with additives ---------- 18

1.3 Device Structure ---------- 21

1.4 Adaptation for tandem ---------- 23

1.5 Transparent Conducting Oxides ---------- 29

1.6 Motivation of the research ---------- 34

1.7 Buffer Layer and metal oxide nanoparticles ---------- 34

II. Experimental Method

2.1 Preparation of perovskite film ---------- 35

2.2 Buffer Layer preparation and deposition ---------- 35

2.3 Transparent Electrode Deposition ---------- 36

2.4 Characterization ---------- 36

III. Results and Discussion

3.1 Zn_2SnO_4 buffer layer ---------- 37

3.2 Device performance with combined buffer layer ---------- 47

IV. Conclusion ---------- 58

V. References ---------- 59

ULSAN NATIONAL INSTITUTE OF
SCIENCE AND TECHNOLOGY

List of Figures

Figure 1. Basic configuration of perovskite ABX_3

Figure 2. Schematic figure of degrades of perovskite solar cell. Carrier recombination process of ETL, moisture dissolution of perovskite

Figure 3. Classification of additives for perovskite devices

Figure 4. Different kinds of perovskite device structures with planar, mesoporous scaffold structure

Figure 5. The Shockley-Queisser limit of solar cells

Figure 6. Solar irradiance spectrum from the sunlight to earth

Figure 7. Schematic illustration of basic operation of perovskite solar cell.

Figure 8. Schematic description of varied tandem devices.

Figure 9. Schematic description of DC magnetron sputtering process

Figure 10. Schematic illustration of RF sputtering process

Figure 11. J-V characteristic of opaque perovskite solar cell with varied buffer layer condition

Figure 12. J-V characteristic of perovskite cell with molybdenum oxide and Au electrode over time.

ULSAN NATIONAL INSTITUTE OF SCIENCE AND TECHNOLOGY

Figure 13. Schematic description of energy diagram of semi-transparent perovskite solar cell

Figure 14. Scanning electron microscopy (SEM) image of Spiro-OMeTAD surface with (a) Zn_2SnO_4 nanoparticles and (b) ZTO/MoO_x buffer layer

Figure 15. TEM images of Zn_2SnO_4 nanoparticles.

Figure 16. X-ray diffraction patterns of Zn_2SnO_4 nanoparticles.

Figure 17. SEM images of semi-transparent perovskite solar cells

Figure 18. X-ray diffraction patterns of pristine perovskite film and perovskites with varied buffer layer and ITO electrode.

Figure 19. UV-vis absorption with different halide anion and organic cation ratio of perovskite

Figure 20. Transmittance spectra of MoO_x buffer layer and sputtered ITO with varied buffer layer conditions.

Figure 21. Semi-transparent perovskite solar cell transmittance spectra with ZTO/MoO_x buffer layer

Figure 22. J-V curves of semi-transparent perovskite device with varied buffer layer conditions measured with a large active area (1.00 cm^2)

Figure 23. J-V curves of semi-transparent perovskite solar cell with varied buffer layer conditions measured with a small active area (0.094 cm^2)

ULSAN NATIONAL INSTITUTE OF
SCIENCE AND TECHNOLOGY

Figure 24. Semi-transparent perovskite solar cell external quantum efficiency spectra with ZTO/MoOx buffer layer

Figure 25. Semi-transparent perovskite solar cell steady state data with ZTO/MoO_x buffer layer

Figure 26. J-V characteristic of best semi-transparent perovskite device

Figure 27. Stability test of semi-transparent perovskite device efficiencies in normal room condition

Figure 28. Stability test of semi-transparent perovskite device efficiencies in 85℃ thermal condition

ULSAN NATIONAL INSTITUTE OF
SCIENCE AND TECHNOLOGY

List of Tables

Table 1. Photovoltaic performances of opaque solar cell in Figure 11.

Table 2. Photovoltaic performances of opaque solar cell in Figure 12.

Table 3. Photovoltaic performances of semi-transparent solar cells in Figure 22

Table 4. Photovoltaic performances of semi-transparent solar cells in Figure 23

ULSAN NATIONAL INSTITUTE OF SCIENCE AND TECHNOLOGY

I. Introduction

1.1 History of perovskite solar cell

Lots of researches had been held related to environmental issues because of the greenhouse effect. The greenhouse effect was caused by the gas which confine the sunlight after reflected from the earth. This generated the higher temperature of the earth and additional abnormal temperature phenomena. Solar cells were one of the studies as alternative plans that absorbs solar energy and convert into the electrical energy. Mostly, solar cells had been made of silicon semiconductor by its long warranty and high performance in low light environments. But silicon semiconductor exhibited weakness of performance by increasing temperature and the fabrication cost was expensive. To reduce the fabrication cost, several materials were investigated to substitute the silicon semiconductor and perovskite was one of the materials emerge by these researches for reducing the costs. Perovskite mineral was firstly discovered by Lev Perovski, mineralogist of Russia, in Ural Mountains of Russia in 1839. Initially, perovskite material was composed to form $CaTiO_3$. The structure was described as a cubic unit cell, which located titanium atoms at the corners, oxygen atoms at the middle of the edges, and a calcium atom at the center. In the description of lattice arrangement of perovskite, the positively charged cation A located at the center of a cube. Then cation B located at the corners of cubic structure. Finally, negatively charged anion were occupied at the faces of cubic structure. The perovskites materials showed the properties of superconductivity which means they could conduct electricity without much resistance, as well as non-conductor-semiconductor-piezoelectric that could be applied to solar cells[1].

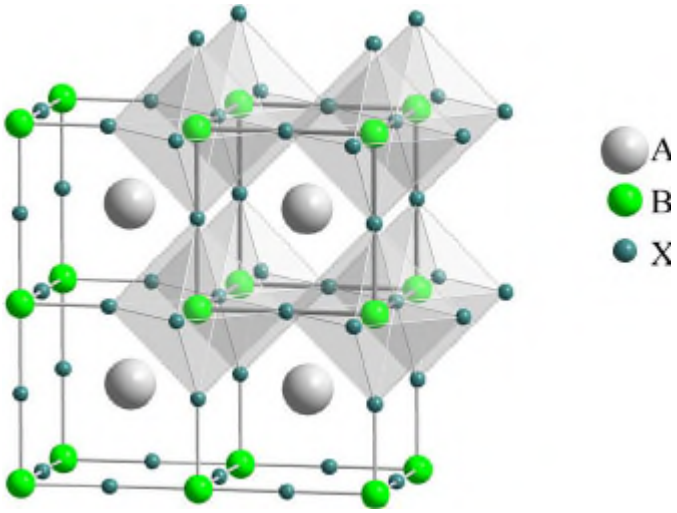

Figure 1. Basic structure of perovskite ABX_3[40].

ULSAN NATIONAL INSTITUTE OF SCIENCE AND TECHNOLOGY

The perovskite materials were firstly used by Tsutomu Miyasaka, electrochemist in Toin yokohama university. They used organic-inorganic hybrid perovskite structure for light absorbing. They reported $CH_3NH_3PbBr_3$ perovskite as an absorbing layer on porous TiO_2[2]. They checked feasibility of perovskite as a light absorbing layer of solar cell with 2.2% of conversion efficiency. Also, they tried to replace the bromide of perovskite to iodine. They coated mesoporous TiO_2 film and dropped the solution of CH_3NH_3I and PbI_2. The result of $TiO_2/CH_3NH_3PbI_3$ layer obtained J_{sc} as 11.0 mA/cm2, V_{oc} as 0.61V, fill factor as 57% with PCE as 3.81%[3]. After, Park and his coworkers used perovskite structures for quantum dots (QDs) on the surfaced treated TiO_2 layer. They claimed that the perovskite showed better absorption than N719 dye sensitizers, which showed 6.5% of its efficiency[4]. But perovskite solar cells had a problem with their rapid degradation because of the solubility of perovskite to the electrolytes. To solve this problem, Park and Gratzel reported solid state spiro-OMeTAD hole transport material (HTM)[5]. With perovskite nanoparticles and spiro-OMeTAD, performance of the device was much increased to 9.7%. Spiro-OMeTAD HTM was also used with perovskite in Snaith's group[6]. With mesostructured solar cell, they reduced the energy losses during charge separation and generated open-circuit voltage (V_{oc}) over 1.1 volts, improving the efficiency to 10.9%. The efficiency of nanostructured perovskite solar cell had jumped to 12.3% by Seok's group[7]. They used band gap engineering process that substituted iodine with bromine. By exchanging 10% of iodine to bromine, more than 10% of average conversion efficiency was improved. Furthermore, substitution of halide to 20% induced higher bandgap, but the solar cell showed greatly improved stability in ambient condition. Without stopping here, Seok's group improved the perovskite solar cell's efficiency to 16.2% with mixed halide composition[8]. They used anti-solvent dropping method with toluene while perovskite solution spin coating to form uniform, dense surface of perovskite.

So far, most inorganic/organic hybrid perovskite solar cells adapted $MAPbI_3$ material. Seok and his coworkers substituted the existing $MAPbI_3$ to formamidinium lead iodide ($FAPbI_3$) perovskite with broad solar absorption spectrum because of its lower band gap[9]. They used intramolecular exchange to fabricate enhanced crystallinity and large grain sizes of perovskite by using DMSO molecules. With DMSO, there was an exchange of DMSO-PbI_2 with FAI to crystalize $FAPbI_3$ and remove DMSO. This showed the improved efficiency to 20.1%. And they tried to control the composition of perovskite with comparatively narrow bandgap formamidinium lead iodide and methylammonium lead bromide[10]. By adding $MAPbBr_3$ into relatively unstable $FAPbI_3$, the perovskite phase was stabilized, and the efficiency was also increased. Efficiency of $MAPbBr_3$ incorporated perovskite was 19.0% with 22.5 of J_{sc}, 1.12 of V_{oc}, 75,7% of fill factor. And they studied about the phenomena of formamidinium and methylammonium lead perovskite grain boundary by Kelvin force microscopy in noncontact/contact modes[11]. They found enhanced ion migrations in grain boundaries rather than grain interior and they induced the morphological changes. It showed the beneficial effects of grain boundaries to perovskite

ULSAN NATIONAL INSTITUTE OF SCIENCE AND TECHNOLOGY

solar cell.

Additionally, Seok's group found the beneficial effects of additional PbI_2 to perovskite solar cells[12]. The excess amount of PbI_2 in organic-inorganic perovskite showed reduced hysteresis with shorter delay time. With the additional PbI_2, the perovskite solar cell recorded 20.1% of efficiency. Also, they used iodide ions to the two-step fabricated perovskite solar cell by adding to the organic cation to reduce defects, which are cause of decreased circuit voltage, current density, and efficiency.[13] The result showed jumped efficiency to 22.6% with much lower hysteresis. So the effects of additional iodide to perovskite were studied by electron-beam-induced current measurements (EBIC)[14]. The result illustrated that amounts of excess iodide decreased the concentration of halide vacancy defects and higher concentration of perovskite carrier inside of the nanostructure. It suggested that these results were related to improved performance.

The perovskite solar cell efficiency was furtherly increased by changing hole conducting layer[15]. The solid state spiro-OMeTAD was substituted by fluorine terminated material because of its poor thermal stability from the additives. With the finely tuned energy level of new DM HTM, the efficiency of the perovskite cell reached 23.2%. And after several improvements, perovskite solar cell efficiency was described to 24.2% on the official chart[16].

Perovskite solar cells had been developed with the lots of experiments and recorded high efficiency. But still, perovskite solar cell has been suffering from several challenges about stability issues for commercialization[17]. The instability issue of perovskite happened in the charge transporting layer and interface degradations. For the electron transportation, TiO_2 has been used commonly but it induced photocatalytic degradation in UV illumination condition. Also, spiro-OMeTAD, PTAA organic materials for hole transportation had thermal and moisture weaknesses. The main reasons of the perovskite cell degradations were oxygen, moisture, light, etc.[18]. For TiO_2 ETL of perovskite device, the superoxide radicals (O_2^-) made by oxygen vacancy of thermally annealed TiO_2 induced formation of the depletion area at the TiO_2 surface. And depletion area made an upward bending of conduction band. Also, UV illumination induced surface trap sites, binding electrons in trapping sites to oxygen molecules, generating Ti^{4+}-O_2^- complex. Additionally, Pb-X complex generated free radicals and then degraded the perovskite to halogens by oxidation. For example, $MAPbI_3$ perovskite with UV illumination broke down and generated PbI_2 molecules.

In the humid environments, possible mechanisms of $MAPbI_3$ decomposition were illustrated by descripted equations[21]. $MAPbI_3$ was firstly decomposed to MAI and PbI_2. Additionally, MAI again decomposed to MA and HI gases.

ULSAN NATIONAL INSTITUTE OF SCIENCE AND TECHNOLOGY

$$CH_3NH_3PbI_3 \overset{H_2O}{\rightleftharpoons} PbI_2 + CH_3NH_3I(aq.)$$

$$CH_3NH_3I(aq.) \rightleftharpoons CH_3NH_2(aq.) + HI(aq.)$$

$$4HI(aq.) + O_2 \rightleftharpoons 2I_2 + 2H_2O$$

$$2HI(aq.) \overset{h\nu}{\rightleftharpoons} H_2\uparrow + I_2$$

$$CH_3NH_3PbI_3 \overset{h\nu}{\rightleftharpoons} PbI_2 + CH_3NH_2\uparrow + HI\uparrow$$

$$2I^- \overset{h\nu}{\rightleftharpoons} I_2 + 2e^-$$

$$3CH_3NH_3^+ \overset{h\nu}{\rightleftharpoons} 3CH_3NH_2\uparrow + 3H^+$$

$$I^- + I_2 + 3H^+ + 2e^- \rightleftharpoons 3HI\uparrow$$

There was another suggestion of degradation of $MAPbI_3$. Leguy reported that the first hydrate of $MAPbI_3$ perovskite was $MAPbI_3 \cdot H_2O$ and it underwent additional hydration with the described equation[19].

$4MAPbI_3 + 4H_2O \rightleftarrows [4MAPbI_3 \cdot H_2O] \rightleftarrows MA4PbI_6 \cdot 2H_2O + 3PbI_2 + 2H_2O$[19]

They claimed that the formation of the first hydrate could be reversible which meant that the perovskite photovoltaic performance could be restored by dehydration process. But with the excess exposure of water, the PbI_2 was generated irreversibly and the perovskite layer could be dissolved. For these stability issues, several researches were experimented to improve the perovskite device stability.

ULSAN NATIONAL INSTITUTE OF SCIENCE AND TECHNOLOGY

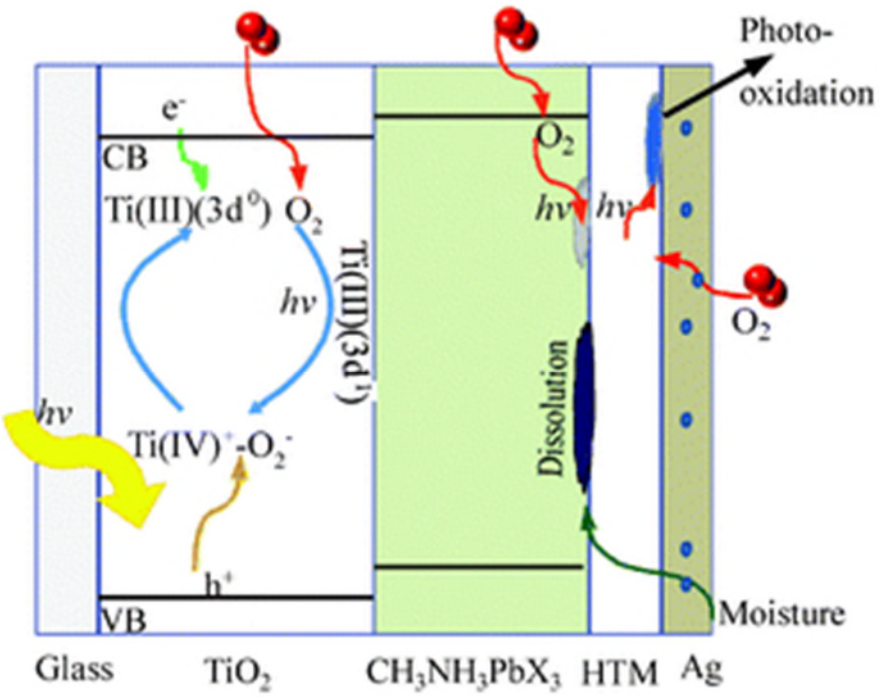

Figure 2. Schematic figure of degradations of perovskite solar cell. Carrier recombination process of ETL, moisture dissolution of perovskite.[18]

ULSAN NATIONAL INSTITUTE OF SCIENCE AND TECHNOLOGY

Firstly, there was a try to substitute the carrier transport layers of solar cells. Jingbi You reported NiO_x and ZnO as a charge transport layer by solution process[20]. To prevent degradation from the ZnO and Al electrode interfaces, they modulated the device structure with inverted construction. By substituting organic layers with inorganic layers, they could diminish the degradations by water and oxygen and retained 90% of its initial efficiency in ambient condition.

In the perovskite composition field, some researchers incorporated cesium cation to perovskite for higher stability. Michael Gratzel used triple mixed Cs/MA/FA cation perovskite[22]. Adding cesium to perovskite decreased the impurities of yellow phase and generated uniform grains with seed assisted crystal growth. The stability of efficiency was reported from 21.1% to 18% after 250 hours under operating condition. The effects of cesium were also checked in the lead-bromide perovskites[23]. By comparing $CsPbBr_3$ with $MAPbBr_3$ on mesoporous TiO_2, $CsPbBr_3$ perovskite showed much improved stability rather than $MAPbBr_3$. Additionally, CsBr was used for modifying the interface between ETL and perovskite film[24]. With the TiO_2 transport layer, CsBr contained perovskite showed improved stability of efficiency and resilience of perovskite to UV exposure. It showed the positive expects to the long-term stability. In the other materials, elemental sulfur in perovskite precursor was reported[25]. The elemental sulfur greatly blocked the degradation of FA/MA mixed precursor due to the deprotonation of methylammonium by amine-sulfur coordination. Although it was found that the sulfur materials were remained in the perovskite film, they did not affect to the perovskite cell efficiency.

For the stability of three-dimensional perovskites, researches about two-dimensional perovskites showed good results about the device stability. Smith and his coworkers reported PEA material to make double layered perovskite by spin-coating[26]. The three-dimensional perovskite with 2D additional layer showed high resistance to the moisture than the pristine structure due to the hydrophobic property of layered perovskite. Additionally, they suggested that the large band gap of 2D perovskite could be used as a large bandgap dual absorber[27]. With the efficiency of 15.3%, they showed the improved stability of perovskite solar cell. Hsinhan Tsai and his group also used 2D structured perovskite for the higher stability[28]. They used Ruddlesden-Popper thin, $(BA)_2(MA)_3Pb_4I_{13}$ layered perovskite film with preferential plane alignment and induced 12.52% of efficiency without hysteresis. Also, the efficiency retained 60% of its initial efficiency after 2,250 hours under light illumination.

ULSAN NATIONAL INSTITUTE OF SCIENCE AND TECHNOLOGY

1.2 Perovskite material tuning with additives

After the emergence of perovskite solar cell by Tsutomu Miyasaka and his group, there were a lot of researches to increase the efficiency of perovskite cell. One of them was adding additives to perovskite. For example, adding halide additives into pristine lead iodide perovskite increased the device performance. In detail, methylammonium chloride (MACl) additive into pristine $MAPbI_3$ improved the crystallization and coverage of the film. By Yixin Zhao and Kai Zhu, adding MACl led to better crystallinity of perovskite with both mesoporous and planar structure[51]. This induced the increased efficiency of planar device from 2% to 12% and mesoporous device from 8% to 10%. And during the thermal annealing process of perovskite film, it was found that amounts of Cl were removed. From this, amounts of other halide excess additives were also reported. Alex K. Y. Jen group added alkyl halide into the perovskite precursor[52]. The alkyl halide chain dissociated the halide ion and made additional halide source for lead ion. They compared I, Br, Cl alkyl halide additives and found that all these additives were successful to improve the pristine perovskite efficiency. They illustrated the mechanism of additives that degraded MA in perovskite precursor reacted with halide additive and released the halide ion for the lattice formation of perovskite. The released halide from additives then made a reaction with Pb^{2+} ion and resulted crystallization of perovskite. Yian Xie and Fuqiang Huang selected MAI additive to PbI_2 precursor to control the crystallization of PbI_2 film on mesoporous structure[53]. By increasing the MAI amounts to some extent to PbI_2 precursor, the grain sizes were increased, and the roughness of PbI_2-MAI film became smooth. But excessive adding of MAI caused increased roughness with degraded efficiency of solar cell. L. Zhao et al. claimed that Br^- additives could control the perovskite morphology[54]. They used MABr as an additive and the crystallinity of perovskite film was maximized with 1.5 mol% of MABr. And unlike MACl, the bromide was remained in perovskite and slightly shift the peak of XRD and UV-vis spectra. It implied that bromide additives could make blue shifts of optical bandgap of perovskite and induced the increase of V_{oc}. The MABr additive also reduced the carrier lifetime of pristine perovskite. This showed that the Br^- additive accelerated the charge extraction in perovskite layer.

Not only the organic halide additives, metal halide additives were also used to improve the crystallinity of perovskite film. Chin Wei C. et al. introduced KCl, NaCl, LiCl metal halide salts as additives in PbI_2 precursor[55]. These metal halide additives changed the morphology of PbI_2 film and increased crystallinity of perovskite. Especially, KCl had a great effect to perovskite crystal sizes and efficiency. Without any additives, the crystal sizes of perovskite were 253±20 nm. But with the KCl additive, the crystal sizes greatly increased to 468±50 nm. And it was known that the larger grain size could minimize the penetration of oxygen and water. Through this property, perovskite with KCl additive showed improved efficiency stability with 80% of its initial value after 50 days. In the impedance spectroscopy,

ULSAN NATIONAL INSTITUTE OF SCIENCE AND TECHNOLOGY

KCl with perovskite showed decreased resistance which indicated reduced trap sites and resistive losses. Michale F. Durstock et al. used sodium ions to PbI_2 precursor solution[56]. They used NaI and NaBr into a DMF solvent. The sodium additives acted as a nucleation site and the resulted perovskite showed larger grain sizes and improved efficiency. As a result, additive added perovskite did not show any impurities like PbI_2 and MAI without peak position shifts[57]. Gratzel and co-workers used monovalent cation halide additives which include NaI, CuBr, CuI, and AgI[58]. Without changing crystal structure of perovskite, additives modified crystal sizes of perovskite with spherical shapes, to result passivation states of perovskite surface. Also, monovalent cation additives increased electron mobility and balanced charge transport which induced high current density. The best efficiency of additive-added perovskite was 15.61%, which was higher than 14.01% of pristine perovskite. In the cases of lead-free perovskites, tin based perovskites such as $CsSnI_3$, $MASnI_3$ were commonly used. However, Sn^{2+} in perovskite could be easily oxidized to Sn^{4+}, which degraded charge extraction and stability issues in ambient condition. Mathews et al. addressed these issues of $CsSnI_3$ lead-free perovskite with SnF_2[59]. By adding SnF_2, the variation of lattice parameters was not shown. It meant that the fluorine ion radii were smaller than that of iodide ion so the substitution from I^- with F^- was not happened. But SnF_2 additive decreased yellow non-perovskite morphology. Also, the current density of $CsSnI_3$ was dramatically improved with the photoelectric effect. Without SnF_2 addition, pristine $CsSnI_3$ perovskite showed bad current density of 0.19 mA/cm^2, while it was increased to 23.5 mA/cm^2 with 20mol% of SnF_2 addition. In the carrier densities, $CsSnI_3$ had high hole carrier densities ~$10^{19}/cm^3$ which were the majority carriers. Such a high p-type carrier density was generated from the Sn vacancies due to the oxidation. Adding SnF_2 could fill the Sn vacancies of perovskite and then decreased the defect densities. As a result, the decreased majority hole carrier and defects made tin-based perovskite as a semiconductor for light harvesting layer of solar cells. So, the modified amounts of metal impurities for perovskite improved the morphology with larger grain sizes, varied crystal orientations, controlled charge carriers, and removed defects.

As the solute additives were actively researched, solvent modulations for perovskite crystallization were also progressed. In the coating process of perovskite, conversion to perovskite from PbI_2 with enough crystal morphology was important. Especially in planar structure, it was hard to control perovskite crystal sizes. When loading MAI solution on PbI_2 pre-deposited layer, the proportion of $MAPbI_3$-PbI_2 was not formed constantly, which meant the reproducibility of the cell was not good. Luyuan Han et al. produced the PbI_2 solution made with DMSO instead of DMF[60]. DMSO solvent indicated stronger coordinate bindings between Pb^{2+} and solvent, which decreased the fast crystallization of PbI_2. As a result, the sequential deposition of perovskite on DMSO based PbI_2 film enabled the centralization of perovskite crystal sizes, which were smaller than that of DMF solvent. The deviation of efficiency was decreased from 2.47 to 0.57%. Kai Zhu et al., added amounts of MAI into PbI_2 precursor to fabricate

ULSAN NATIONAL INSTITUTE OF SCIENCE AND TECHNOLOGY

10 folds faster perovskite formation without any remains of PbI_2 defects on perovskite film[61]. With increased absorption spectra and sequent deposition step, the cell efficiency was improved from 6.11% to 17.22%. Ce Hao and coworkers added small amounts of TBP into DMF-PbI_2 precursor to deposit porous layer of randomly packed PbI_2 crystals[62]. The nitrogen atom from TBP induced stronger tendency to Pb ion to change the crystallization. And TBP itself could be a dispersing agent for perovskite morphology. The porous PbI_2 film showed 80% of transmittance from incident light, which illustrated the difference of porous and compact film. But after the second deposition of perovskite film, the absorbance of film induced by TBP was much higher than the pristine condition. Yue Hao et al. modulated the MAI solvent for two-step deposition by adding DMF into MAI-IPA solution[63]. With DMF addition, the perovskite grain sizes were increased, and the pinholes located in grain boundaries which induced recombination problem with degraded efficiency were removed. Also, the solvent addition to IPA erased the PbI_2 defects on perovskite surface and increased the crystallinity of perovskite. These results were illustrated that DMF made the IPA penetrate the PbI_2 film deeper and increase the domain size.

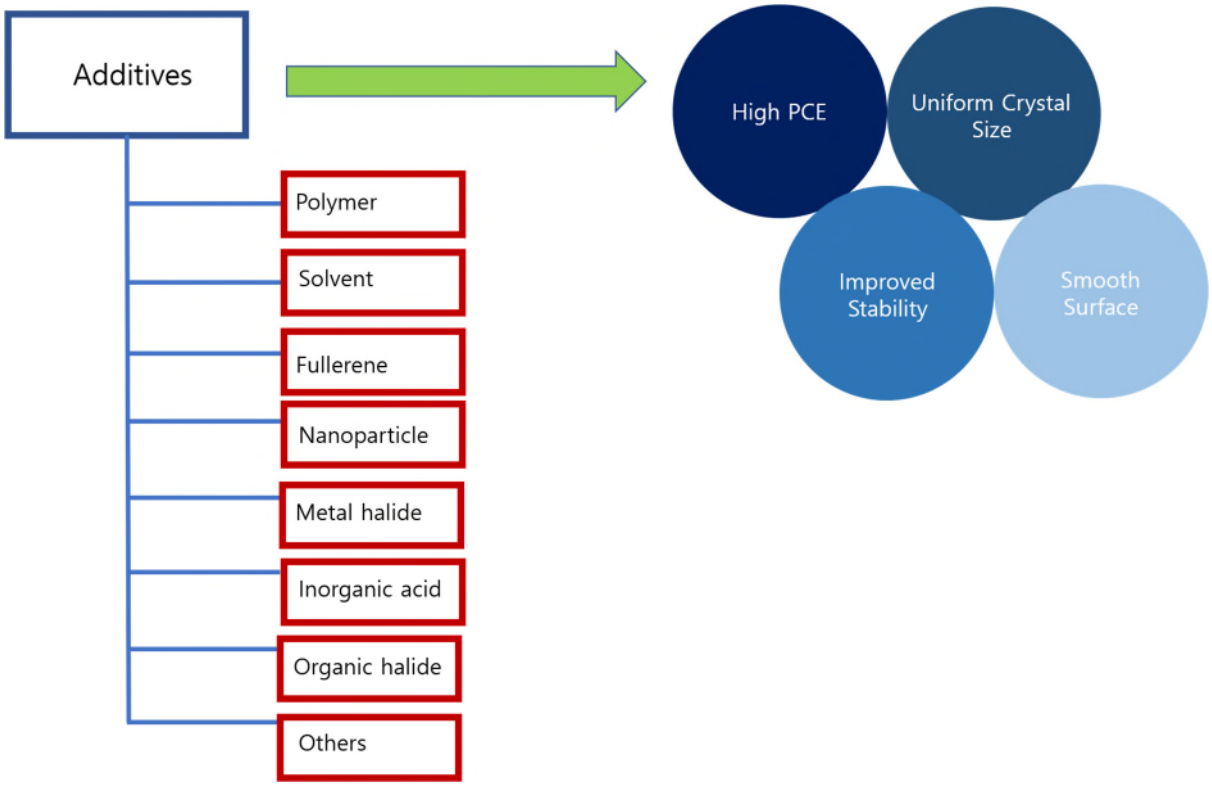

Figure 3. Classification of additives for perovskite solar cells[66].

ULSAN NATIONAL INSTITUTE OF SCIENCE AND TECHNOLOGY

1.3 Device Structure

Commonly, the structures of perovskite solar cells could be divided in two types. One was containing mesoporous electron transporting layer with shorter carrier transport time when the light was absorbed in perovskite and separate carriers. Normally mesoporous structure was composed with compact TiO_2/mesoporous TiO_2/perovskite/hole collection layer which generated the electron transport from perovskite to mesoporous electron collecting layer. And in a planar structure, perovskite located between electron and hole transport layer without mesoporous layer. Planar structure had an advantage as it was simple to fabricate rather than mesoporous structure because it did not need additional tuning of scaffold and high thermal annealing process. Also, with the mesoporous ETL, the thickness of mesoporous ETL/perovskite layer was thicker than planar structure and this thickness was related to the transparency when it was applied to tandem structure. In a single junction case, current density and V_{oc} could be modulated by controlling thickness of charge separation/transmission layer. And the thickness of perovskite was thick enough to absorb as much as possible solar energy. But in the multijunction structure, thicker perovskite than other layers should be avoided. If a thickness of one subcell was too thick, the other subcell could not receive enough solar energy and did not generate amounts of charge separations, inducing low efficiency. So, matching the thickness of each subcell into a tandem design was important. To transmit the sunlight to rear subcell, the thickness of perovskite and charge transport layer of front subcell should have been thin. By this, planar perovskite structure was preferred with thin ETL/perovskite layer in application for tandem design.

ULSAN NATIONAL INSTITUTE OF
SCIENCE AND TECHNOLOGY

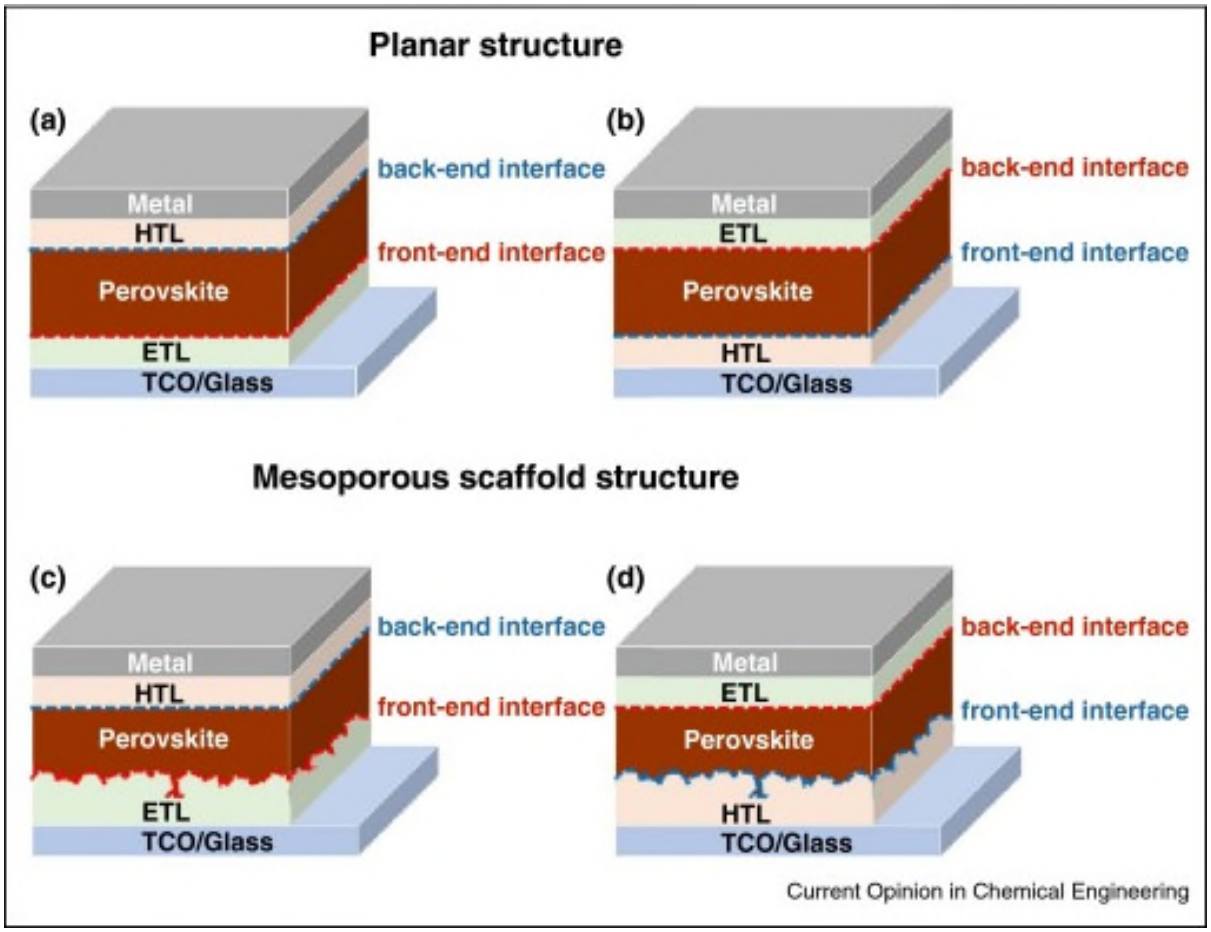

Figure 4. Different kinds of perovskite solar cell structures with planar, mesoporous scaffold structure[67]

ULSAN NATIONAL INSTITUTE OF SCIENCE AND TECHNOLOGY

1.4 Adaptation for tandem

Although the efficiency of perovskite was very high, Shockley and Queisser illustrated calculated limitation of PCE. Figure 5. illustrated the theoretical maximum efficiency of single junction was around 33.7% under AM 1.5 solar spectrum. By researching the topic of higher efficiency regardless of the Schockley-Queisser limit, multijunction solar cell rose to the surface. Multijunction, tandem structure was a method to divide the solar spectrum and optimize the absorb wavelength regions. In the case of single junction with certain bandgap, the semiconductor could absorb part of the solar radiation spectrum (Figure 6.), Multijunction solar cell targeted this property that each single junction could separate the absorption wavelength area and optimize the amount of spectrum absorbed. There were several kinds of tandem structure illustrated in figure 8. First structure was mechanically stacked 4-terminal tandem. The structure was made of two independently fabricated subcells and individually connected. This 4-terminal tandem structure was the simplest device to fabricate because it did not require additional techniques of connecting two subcells, because it just contacted them individually. Also, 4-terminal tandem did not require current matching, meant that each subcell could use optimized fabrication process. But the problem was it increased the cost by doubling electric power. One of the solutions was parallelly connected 2-terminal structure. The two subcells were monolithically stacked containing recombination layer between two subcells. It reduced the fabrication costs with less construction process and parasitic absorption in nonactive layer.

Initially, perovskite was usually combined with silicon semiconductor. To absorb the spectrum in different wavelength region, the band gap should have been spread to optimize the solar absorption. Perovskites were firstly used for tandem in 2014. Philipp Loper used $MAPbI_3$ top subcell with c-Si heterojunction bottom cell in 4-terminal tandem structure[29]. The perovskite top cell showed more than 55% of the transparency in NIR region with 13.4% of 4-terminal tandem efficiency. In 2015, the efficiency of 4-terminal tandem with $MAPbI_3$ and c-Si heterojunction was increased by using sputtered IZO transparent electrode of semi-transparent subcell[30]. The Duong tried to advance the semi-transparent solar cell with optimizing the both sides of electrodes of ITO[31]. The perovskite subcell showed over 12% of its efficiency and the transmittance of near-infrared area with over 80%. The efficiency of this 4-terminal tandem cell recorded 20.1%. Additionally, Jinsong Huang reported the higher efficiency of perovskite/c-Si 4-termianl tandem cell by tuning the electrode of semi-transparent perovskite subcell with thin Cu/Au metal electrode[32]. The increased efficiency of perovskite subcell was 16.5% and the final efficiency of tandem device was 23%. The efficiency of perovskite/silicon 4-terminal tandem was further increased to 25.2%[33]. Jeremie Werner compared the 4-terminal and monolithic stacked tandem device by modulation of active area. On the 4-terminal tandem, the efficiencies of full device showed 23% and 25.2% with 1.015 cm^2 and 0.25 cm^2 of device. And on monolithically stacked device, the 1.43 cm^2 of active area induced 20.5% of device efficiency. In 2016,

ULSAN NATIONAL INSTITUTE OF SCIENCE AND TECHNOLOGY

the commonly used $MAPbI_3$ perovskite for 4-terminal tandem was substituted by bandgap tuned perovskite containing cesium[34]. The cesium contained perovskite with 1.63 eV of its bandgap was coated on the indium doped TiO_2 ETL. The indium doped TiO_2 showed improved conductivity in the interface between ETL and perovskite. The efficiencies of semi-transparent subcell and 4-terminal tandem cell with silicon showed 16.6% and 24.5%. Furthermore, The Duong modified the perovskite with triple cation Cs/MA/FA by addition of rubidium[35]. The Rb contained perovskite with 1.73 eV showed improved light stability, the semi-transparent device showed 84% of transmittance between 720 and 1100 nm of wavelength with 16% of efficiency. The 4-terminal tandem cell with interdigitated back contact silicon subcell showed 26.4% of its efficiency.

For monolithic tandem structure, Jonathan fabricated monolithic tandem solar cell with silicon tunnel junction[36]. They reported 13.7% efficiency with 1.65 V of V_{oc}. In the same year, Jeremie reported the monolithic tandem structure over 20% of its efficiency[37]. With the 14.5% efficiency by low temperature process and IZO recombination layer, efficiencies of tandem device showed 21.2% and 19.2% with divided active area, 0.17 and 1.22 cm^2. Furthermore, by adding cesium cation to perovskite, perovskite/silicon monolithic tandem showed 23.6% efficiency with improved stability in 2017[38]. They used SnO_2 buffer layer for ITO sputtering. With $1cm^2$ active area, the efficiency of tandem device maintained its initial efficiency for 1,000 hours.

With the researches about perovskite/silicon tandem devices, there were experiments about the tandem devices entirely made with perovskites. G. E. Eperon illustrated perovskite/perovskite tandem device with divided energy gaps[39]. They serially stacked both devices with changed band gaps of perovskite subcells. Perovskite structure usually conformed with organic-inorganic hybrid cation and halide/oxide anion, ABX_3 structure. The perovskite band gap could be changed by kinds of the composition materials. In organic site, CH_3NH_3 and $NH_3CH_2NH_3$ were commonly used materials and by changing the material from CH_3NH_3 to bigger size one, the band gap was decreased. In the halide site, $I^- < Br^- < Cl^-$ with smaller size induced higher band gap of perovskite. Eperon also used this method to control the band gap. They substituted the inorganic lead site with tin for lower band gap, and mixed bromide and iodide for larger band gap of perovskite. The efficiency of the series connected tandem cell was 17%. Starting with this research, several researches of perovskite/perovskite tandem device were researched. Rajagopal and coworkers tried to fabricate perovskite-perovskite tandem cell with minimizing V_{oc} loss[41]. They added fullerene additive to optimize interfacial connection to increase the V_{oc} of low band gap perovskite cell to 0.84 V. The efficiency of perovskite tandem device showed 18.5% with approaching 80% of theoretical limitation. David F., Henk J. Bolink group fabricated monolithic perovskite/perovskite tandem cell[42]. They also controlled the perovskite band gap to increase the absorption spectrum. For the wide band gap perovskite, they added cesium and bromide to $FAPbI_3$ as an absorber. They used $Cs_{0.15}FA_{0.85}Pb(I_{0.3}Br_{0.7})_3$ perovskite for wide band gap and $MAPbI_3$ perovskite for narrow band gap. For

ULSAN NATIONAL INSTITUTE OF SCIENCE AND TECHNOLOGY

the recombination layer, p-doped TaTm:F6-TCNNQ and n-doped C_{60}:PhIm were selected. And because of the challenge of construction, they just fabricate the wide band gap perovskite and ETL by solution processing method. The remained narrow band gap parts for tandem device were all deposited by evaporation. To make the tandem cell more convenient, there was a research to try to substitute interconnect recombination layer from ITO metal oxide to organic layer of spiro-OMeTAD/PEDOT: PSS/PEI/PCBM: PEI[43]. Generally, transparent conducting layer was coated through magnetron sputtering method. But by the developed organic interlayer, perovskite tandem cell was fabricated by solution process entirely. But the efficiency was not high because they used same $MAPbI_3$ perovskite for top/bottom device. The total efficiency of the tandem cell was 7%, with V_{oc} of 1.89 V. Structural tuning of tandem was also developed because of the fabrication challenge after charge recombination layer. Dewei Z., Changlei W., and Yanfa Y group fabricated 4-terminal perovskite tandem cell using different band gap of perovskite[44]. They just coated charge recombination layer MoOx/ITO on the wide band gap perovskite subcell. The total efficiency of 4-T tandem device was 23.1% with 15.7% of wide band gap device and 7.4% of filtered low band gap device.

ULSAN NATIONAL INSTITUTE OF SCIENCE AND TECHNOLOGY

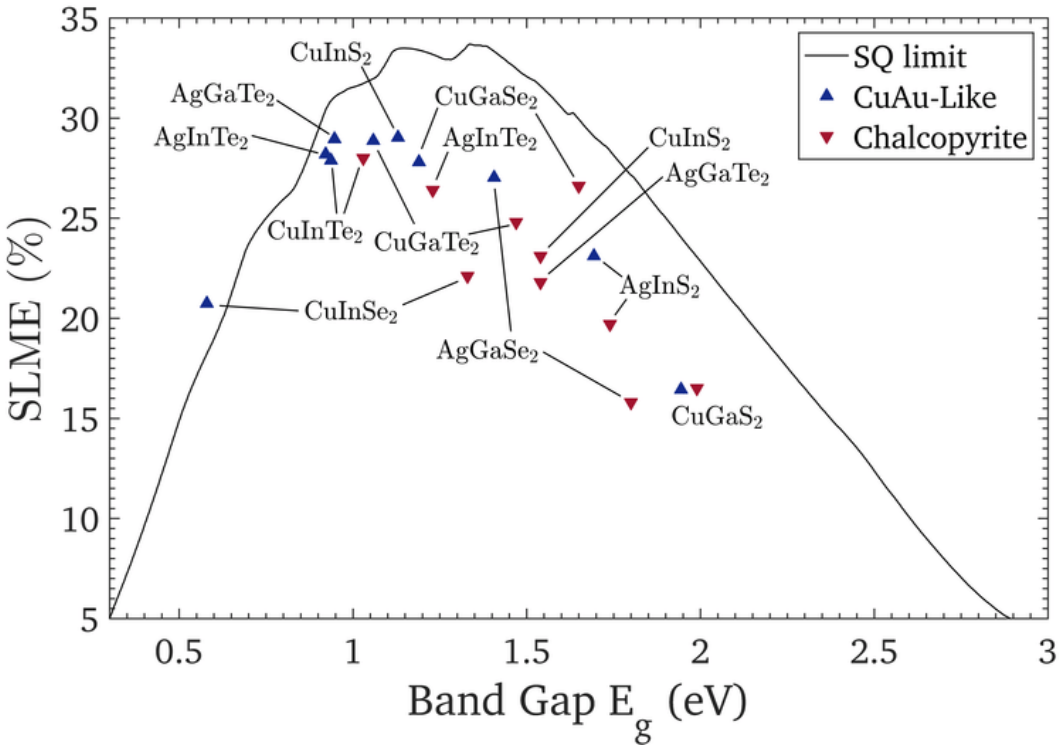

Figure 5. Shockley-Queisser limit (SQ limit) for the solar cell efficiency.

ULSAN NATIONAL INSTITUTE OF
SCIENCE AND TECHNOLOGY

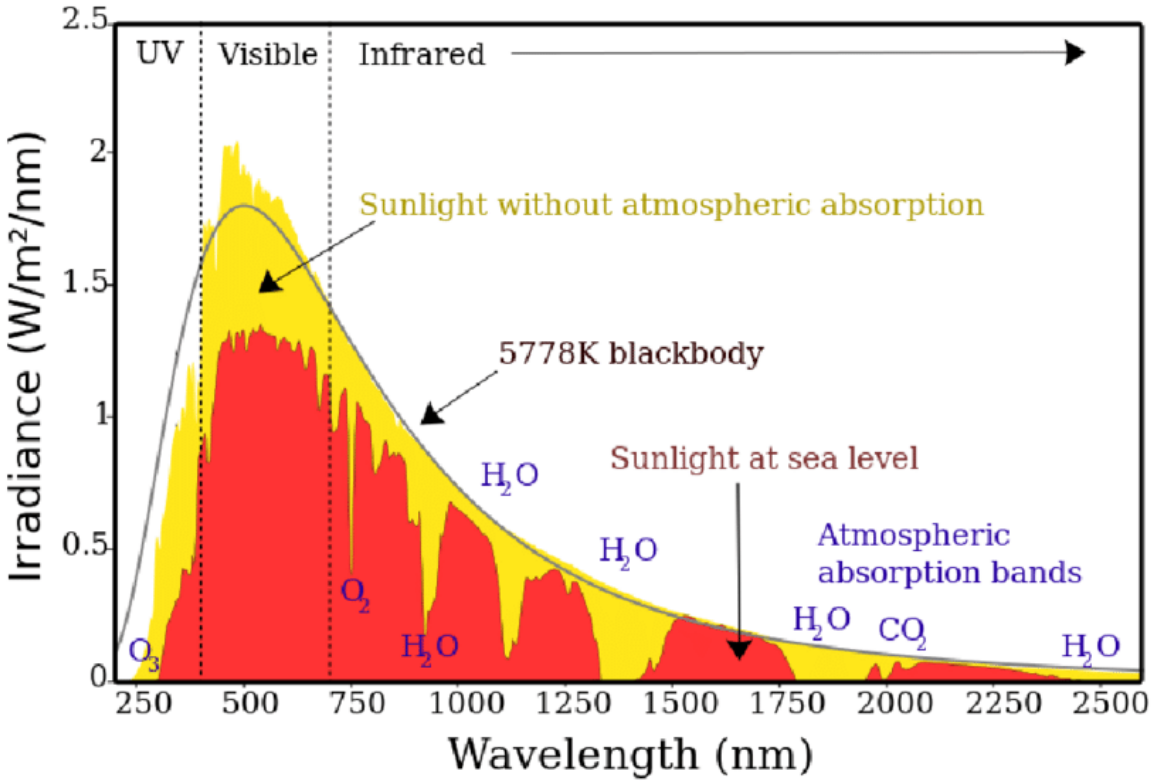

Figure 6. Solar irradiance spectrum from the sunlight to earth

ULSAN NATIONAL INSTITUTE OF SCIENCE AND TECHNOLOGY

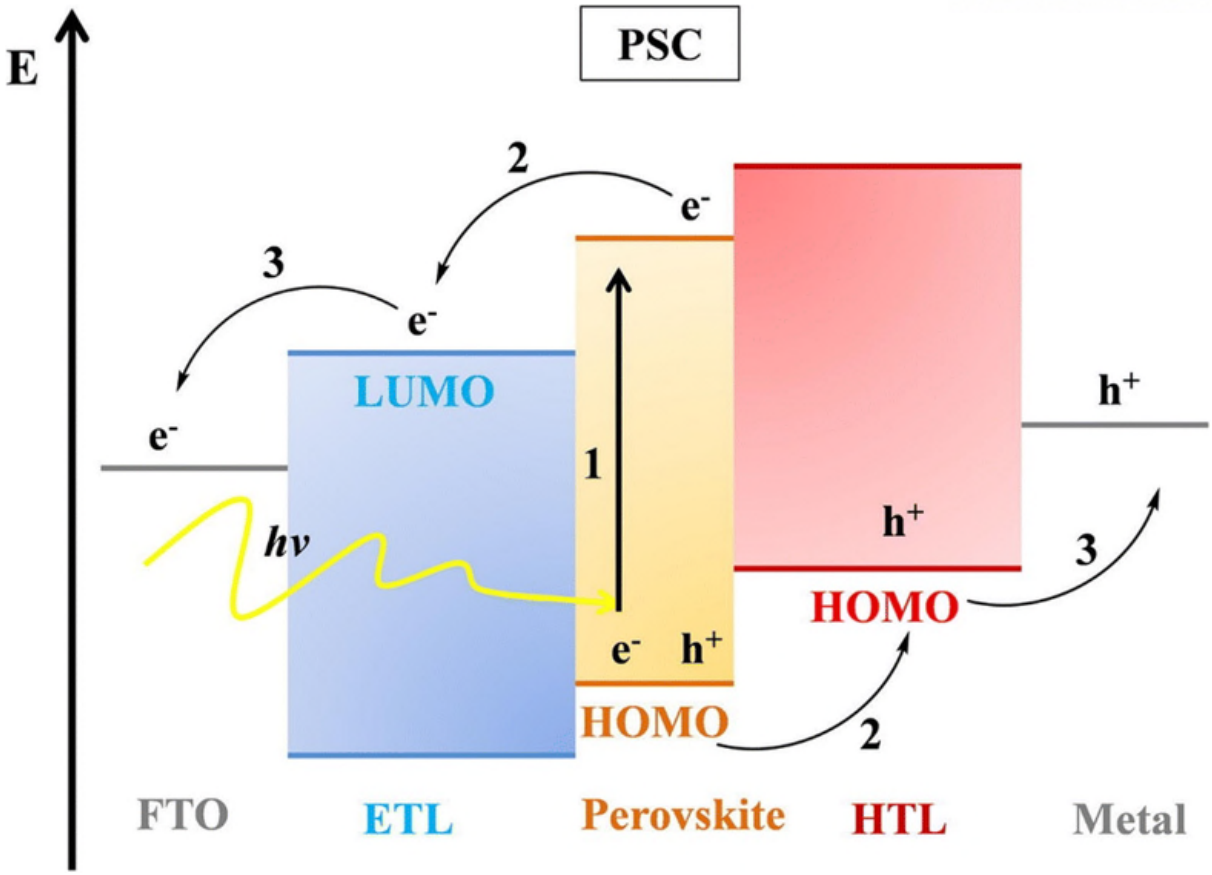

Figure 7. Schematic illustration of basic operation of perovskite solar cell.

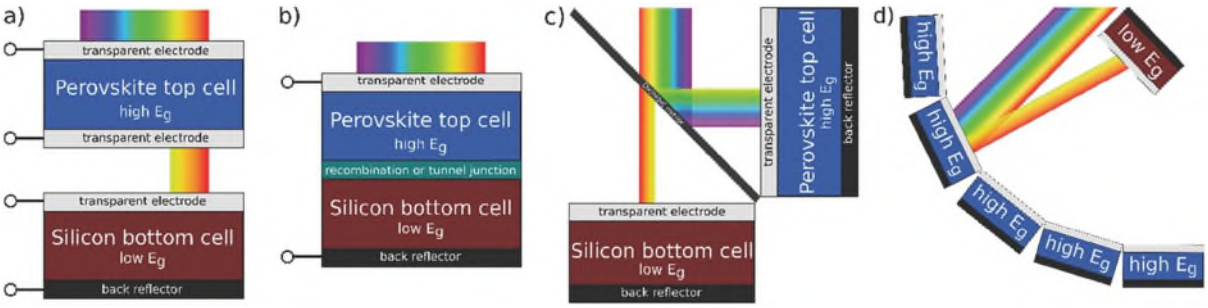

Figure 8. Schematic descriptions of varied tandem device structures.

ULSAN NATIONAL INSTITUTE OF SCIENCE AND TECHNOLOGY

1.5 Transparent Conducting Oxide electrode

In the history of TCO, it was started by thinly depositing Ag or Pt on the front electrode in solar cells in the 1880s. TCO was good to be used as electrodes with good transparency when the sunlight should pass completely through the front electrode. Also, electrons and holes generated by the sunlight should have good electrical conductivity to operate effectively as solar cells. For TCOs, the optical transparency should be more than 80% and at the same time, satisfy $\rho \leq 10^{-3}$ Ωcm of conductivity. To get the transparency over 80%, the energy band gap should be 3.5 eV or more. If a band gap over the visible light region was needed, the energy of the band gap would be insufficient, and a large amount would be transmitted. There were various TCO materials. Among them, ZnO, In_2O_3, MgO and SnO_2 were typical with a band gap 3.5 eV or more. ITO was the mostly used TCO in the industry today. ITO meant indium oxide (In_2O_3) was doped with tin oxide (SnO_2) by 5~10%. The fabricated ITO had an enough band gap for conducting with good work function. So, for fabrication of semi-transparent device, we adopted indium tin oxide (ITO, 10% SnO_2 contained) as an electrode.

For the ITO electrode coating, the magnetron sputtering method was commonly used. The sputtering was a process that ejecting atoms from a sputtering target to the substrate surface. In this plasma environments, free electrons moved from the negatively charged target source. Then these gas atoms turned to positively charged atoms. These positively charged gas ions were greatly dragged to the target surface with high speed. With the high momentum, the particles of target surface were sputtered off and the vacuum chamber. Sputtering of the target atoms happened with the enough kinetic energy of atoms, much higher than thermal energy in plasma environments. For the charged particles, magnetic field was used to control the velocity and behavior of ions. John S. Chapin was recognized for inventing the magnetron sputtering source in 1974. It showed slow and effective small substrate, while common sputtering processes deposited greatly thin films down to the atomic size. The magnetron sputtering used a magnet to trap electrons over the target which were negatively charged. This allowed faster deposition rates because the trapped electrons were not free to bombard.

For magnetron sputtering, there were several kinds of process for the bombardment of the atoms from the target.[65] The basic method of magnetron sputtering was direct current (DC) sputtering. The configuration of DC sputtering system was parallelly located target source and substrate in vacuum chamber. The inert gas in vacuum chamber was usually argon because it had an ability to converse kinetic energy to molecular collision energy in plasma condition which induced driving force of film sputter. For sputtering process of ionized gas atom driven to the substrate, DC sputtering used magnets on the backside of cathode for trapping electrons over the charged target to make the deposition rates faster. DC sputtering method showed economic benefits of metal coating. But it had limitations that deposition of non-conducting insulating materials induced quality issues such as arcing, poisoning of

ULSAN NATIONAL INSTITUTE OF SCIENCE AND TECHNOLOGY

target. Radio frequency (RF) sputtering process was alternating the current's electrical potential in radio frequencies to block the charge building on sputtering target materials. RF sputtering process ran at energetic wave in vacuum chamber with inert gas, same as DC sputtering. It also used magnets on the backside of the cathode and trapped the electrons, not free to bombard. And at the surface of target, positively charged ions were produced and the positive charge built up and led to the succession of sputtering. By alternating the potential while RF sputtering, the target surface could be cleaned by the charge buildup. With RF sputtering, there were several advantages. For example, the plasma in RF sputtering defused through the vacuum chamber rather than concentrating around the target or substrate, which was the property of DC sputtering. Also, RF sputtering maintained plasma environment with lower inert gas pressure. It resulted much less gas collisions and higher efficient deposition on the substrate. By the cleaning process from charge building in each cycle, arching which was related to the quality issues of thin film on surface greatly reduced. In the magnetron sputtering condition, circular pattern was etched into the target surface because of the circular magnetic field. But with the RF sputtering, the width and depth of the race-track were decreased by the AC property of RF discharge with confined electrons by magnetic field. The plasma of RF sputtering produced larger and wider race-track which made uniform and efficient target coating. And in the coating process of insulates to the substrate which induced a charge as with DC sputtering, there was no disappearing anode effect in RF sputtering condition. With a smaller size and higher kinetic energy electrons, the surfaces of substrates developed a charge in plasma environment. Bu there were also disadvantages existed. By the power modulation of AC ratio frequency, the coated materials did not show great charge buildup by being discharged each half cycle and becoming insulate. While RF magnetron sputtering, the magnetic field induced boundary tunnel with trapping electrons near the target, allowing higher current with lower gas pressure that induces even faster deposition rate. And because RF sputtering required radio waves, deposition rates were much slower and it required higher voltages, inducing an overheating and expenses problems.

In our experiments, we used RF magnetron sputtering method for coating low resistance and high transmission oxide layer in visible region. We deposited ITO electrode right on the organic hole transfer layer. But during the magnetron sputtering process, organic hole transport layer received a damage, induced J-V curve degradation. According to Hiroyuki et al, device's J-V curve was greatly degraded by the ITO sputtering time especially in fill factor. The ITO sputtering without any buffer layer resulted additional diode in the circuit and shrinkage. So, to overcome the degradation effect from magnetron sputtering process, additional interlayer between organic hole conductor and ITO was necessary. In most cases of semi-transparent devices in n-i-p structure, molybdenum oxide (MoO_x, $2<x<3$) was commonly used as a buffer layer to block the plasma damage. MoO_x was coated by thermal evaporation before ITO sputtering process. After ITO sputter, we evaporated gold grid at the edge of the electrode

ULSAN NATIONAL INSTITUTE OF SCIENCE AND TECHNOLOGY

for better conductivity of solar cell. The device with MoO_x interlayer showed higher performance of semi-transparent perovskite solar cell rather than pristine device. The efficiency was increased with higher V_{oc} and fill factor. But the MoO_3 surface can be easily reduced, forming MoO_2, inducing small increase of interface recombination[69]. Additionally, MoO_x induced stability problem with the interface effect between MoO_x and gold grid, degraded the device stability in both ambient and thermal atmosphere condition[68]. Also, we found that in the opaque device with MoO_x/Au layer, the stability of the cell was degraded with the efficiency of < 0.1%. According to Erin et al, the MoO_x contained device had selective effect with different metal electrode. It was illustrated that with gold or silver electrode after MoO_x evaporation, the initial device performances did not have much differences. But the efficiencies were dramatically decreased after 24hours, compared to Al electrode. They suggested that Al electrode had a reaction with MoO_x film by relative formation enthalpy, resulting Al_2O_3 additional interlayer, while Au and Ag did not have any reaction with MoO_x. This Al_2O_3 behaved as a physical barrier, blocking the possibility of defects by moisture.

ULSAN NATIONAL INSTITUTE OF
SCIENCE AND TECHNOLOGY

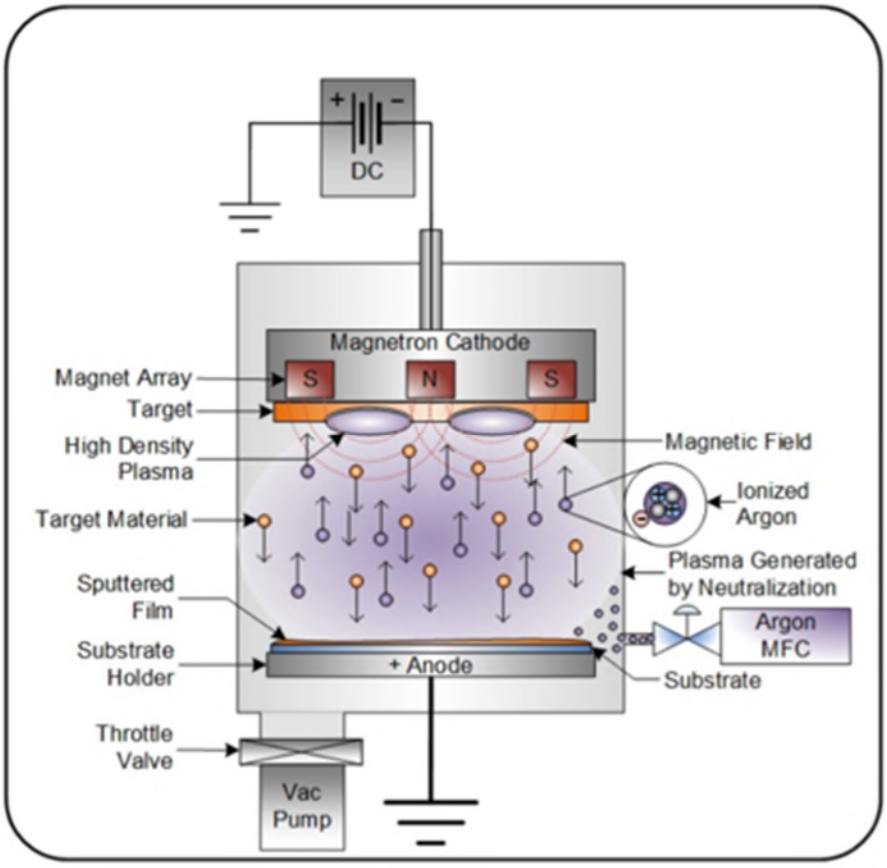

Figure 9. Schematic description of DC magnetron sputtering process

ULSAN NATIONAL INSTITUTE OF SCIENCE AND TECHNOLOGY

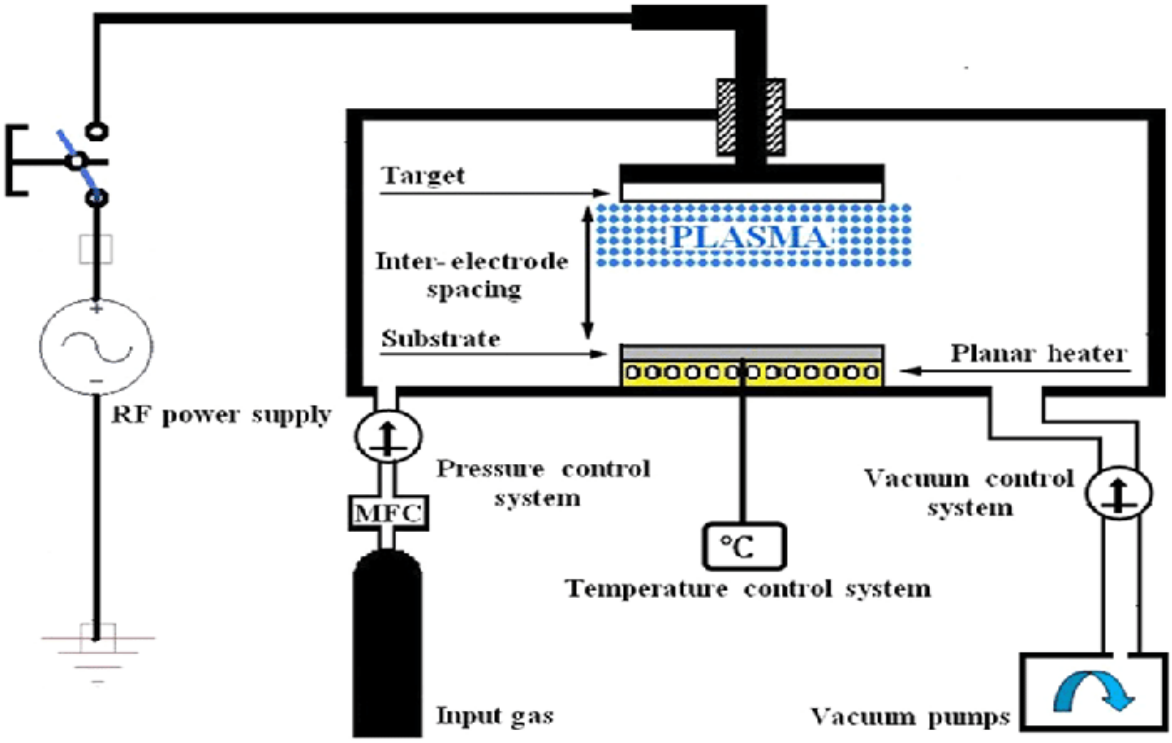

Figure 10. Schematic illustration of RF sputtering process

ULSAN NATIONAL INSTITUTE OF SCIENCE AND TECHNOLOGY

1.6 Motivation of the experiment

Perovskite structure showed good impacts to solar cells. Also, it would be proper to boost solar cell efficiency when applied to multijunction structure. For applying perovskite structure for tandem device, controlling a band gap of perovskite was essential. Additionally, when design the structure of tandem, its charge recombination layer between two subcell was important. The optimum perovskite band gap for tandem device was known as 1.75 eV for absorption spectrum. And during the TCO sputtering process, buffer layers for reducing plasma damage to organic transfer layer were necessary in both subcell stacking systems. Mostly used buffer material in n-i-p structure was MoO_x which induce much higher performance of semi-transparent perovskite solar cell than pristine condition. But it had an issue about its hygroscopic property which absorbs moisture, affected to the stability of the device performance. For fabricating semi-transparent perovskite solar cell with certain stability, we tried to focus on how we modulate transparent electrode and buffer layer.

1.7 Buffer Layer and metal oxide nanoparticles

In the n-i-p semi-transparent perovskite device structure with TCO sputtering progress, MoO_x was mostly used buffer layer to eliminate magnetron plasma damage to organic hole transport layer and perovskite while TCO deposition. Using MoO_x interlayer brought some advantages to higher device performance with increased fill factor, but it was slightly lower than using metal electrode on the organic hole conductor. Same as p-i-n structure, TCO magnetron sputtering induced plasma damage into the organic electron collecting layer (PCBM). To reduce the degradation of organic layer in p-i-n structure, metal oxide materials were used such as aluminum doped zinc oxide (AZO), zinc oxide (ZnO), and others. But different with the MoO_x, metal oxide materials required much higher temperature annealing process for coating. This might induce additional annealing effect to the organic/perovskite layer. Because of this problem, Kevin A. et al explained solution process coating method of metal oxide layer before TCO deposition. They used dispersed nanoparticles of metal oxide (AZO nanoparticles dispersed in IPA) as a buffer layer between PCBM and ITO. By spin coating the nanoparticles, the damage from ITO sputtering was greatly reduced. Also, when the nanoparticle layer was removed in opaque structure, the thermal stability of the cell rapidly degraded, whereas semi-transparent structure with metal oxide nanoparticle layer maintained better thermal stability. This shows that metal oxide nanoparticle layer acted as an insulating layer to prevent degradation of perovskite device.

ULSAN NATIONAL INSTITUTE OF SCIENCE AND TECHNOLOGY

Ⅱ. Experimental Method

2.1 Fabrication of perovskite film

Fabrication of device: Patterned fluorine doped tin oxide glass (FTO glass, TEC8, 8 Ω/cm^2) was cleaned in ultra-sonication with ethanol for 30 mins. Tin isopropoxide precursor (Alfa Aesar) in isopropanol (IPA) was diluted in IPA of 1:10 volume ratio then coated by spin-coating on FTO glass at 3000 rpm. The FTO glasses were then annealed on the hotplate at 250°C for 15 mins. 0.72 mmol $FAPbI_3$ and 0.18mmol $MAPbBr_3$ perovskite powders were dissolved in 0.6ml of N, N-Dimethylformamide (DMF) and 0.3ml of DMSO complex solvent. Perovskite precursor then stirred in 60°C for 30 mins. The 80 ul of the perovskite precursor was loaded and coated at 5000rpm and after 10 s of spin coating, 1ml of ethylene ether was dropped. After finishing the coating, perovskite was annealed on 100°C hot plate for 30 mins. A Spiro-OMeTAD dissolved in chlorobenzene (C.B) of 91.4mg/ml then coated by spin-coating for 3000 rpm 30 s.

2.2 Buffer Layer deposition

Preparation of Zn_2SnO_4: The Zn_2SnO_4 nanoparticles were fabricated in hydrothermal method. 12.8 mmol of $ZnCl_4$ and 6.4 mmol of $SnCl{\cdot}5H_2O$ were dissolved in 200ml of D.I water. $N_2H_4{\cdot}H_2O$ (N_2H_4 molar ratio/Zn = 8:1) was dropped to the solution. The white solution after dropping were moved to th e Teflon-lined autoclave and kept 180°C for 12 hours. The Zn_2SnO_4 nanoparticle precipitates wer e collected and washed by dispersing in D.I water and EtOH for several times. After few ti mes of washing, the particles were finally dispersed in IPA.

In case of opaque device, 70nm of Au was thermally evaporated on HTL without additional buffer lay er. The Au electrode was coated through patterned mask with the 0.094 cm^2 of area. For semi-transparent device, ZnO (Sigma) or AZO (Sigma) or Zn_2SnO_4 nanoparticle ink dispersed in IPA were spin-coated on HTL. Before coating Zn_2SnO_4 nanoparticles, the dispersed precursor of Zn_2SnO_4 was ultra-sonicated about 30 mins. The ZnO or AZO or Zn_2SnO_4 precursor then spin-coated at 4000rpm 60 s. Coated ZnO and AZO and Zn_2SnO_4 films were then dried after spin-coatin g at 75°C for 5 mins.

The MoO_x thin film was deposited by thermal evaporation method. Amounts of MoO_x powder were put in the evaporation boat and then the thickness of MoO_x was controlled manually to reach about 7nm.

ULSAN NATIONAL INSTITUTE OF SCIENCE AND TECHNOLOGY

2.3 Transparent Electrode deposition

We chose indium tin oxide material as the electrode of semi-transparent perovskite cell. ITO was coated by magnetron plasma sputtering process. The type of magnetron sputtering was radio frequency for uniform coating of metal oxide layer. ITO was sputtered at 150W of power with 1mTorr of Ar. Finally, we deposited the metal oxide about 30 mins.

2.4 Characterization

The J-V curves of solar device performance were drawn by a solar simulator (Newport, Oriel Class A, 91195A), which contains a source meter (Keithley 2400) at 100 mA/cm^2 illumination AM 1.5G. Absorption and transmittance spectral analysis were measured by UV-vis spectrometer (Jasco V-780). Morphology and cross-sectional image of sample were checked by Cold FE-SEM (Hitachi, S-4800). The EQE spectra measurement was operated by internal quantum efficiency system (Oriel, IQE 200B). Steady state of sample was characterized with Autolab (Metrohm) instrument. Particle size of Zn_2SnO_4 was measured by normal TEM (JEM-2100). The composition and structure were measured by XRD (Rigaku D/Max 2500V X-ray diffractometer).

ULSAN NATIONAL INSTITUTE OF SCIENCE AND TECHNOLOGY

III. Results and Discussion

3.1 Zn_2SnO_4 buffer layer

In previous reports, Zn_2SnO_4 nanoparticles were dispersed in ethanol for solution progress as electron transport layer. But the solubility of ethanol was concerned because of solubility of ethanol which dissolved perovskite and hole conduction layer when it was spin-coated on spiro-OMeTAD. So, we tried to change the solvent for dispersing Zn_2SnO_4 to block the melting problem. We selected isopropanol (IPA) as a disperse solvent because the solubility of isopropanol was much lower than ethanol for both perovskite and HTL. Also, other metal oxide nanoparticles (ZnO and AZO) were dispersed in isopropanol and used as a buffer layer. The results when Zn_2SnO_4 nanoparticles were dispersed in IPA and spin-coated did not show harmful effects to perovskite and hole transfer layer. And we tested the feasibility of metal oxide nanoparticles as an additional interlayer in opaque structure. ZnO, AZO, and Zn_2SnO_4 were spin-coated on spiro-OMeTAD. After drying the disperse solvent of nanoparticles, Au electrode was thermally evaporated on the interlayer. Figure 11 illustrated J-V characteristics of opaque device with varied interlayers. Configuration of device included SnO_2/perovskite/spiro-OMeTAD/Au and additional interlayer between hole transfer layer and electrode. Each curve showed J-V characteristics of device performance of 1.65 eV band gap perovskite with different interlayer conditions. The pristine perovskite device showed 17.79% of efficiency with J_{sc} of 19.1 mA/cm^2, V_{oc} of 1.16 V, fill factor of 80.4%. ZnO and AZO showed inferior performances with degraded V_{oc} and fill factor. They showed the efficiency over 15%, prominently lower than the pristine structure. But with Zn_2SnO_4 interlayer, the device showed the efficiency within the error range, not much degraded than pristine condition. Device with Zn_2SnO_4 interlayer showed higher V_{oc} and fill factor than other interlayer conditions and the current density value remained as acceptable value.

The figure 13 was the energy diagrams of perovskite device with additional interlayer. Generally, ZnO, AZO, and Zn_2SnO_4 materials were normally used as n-type electron transfer layers. In our structure, we adapted these n-type materials as interlayers between p-type hole conductor and Au electrode. But for the maximum efficiency, matching electronic energy alignment with minimized energy loss was important. When the perovskite active area received solar energy, the charges would be separated into the electron and hole and then each carrier should be separately extracted as electron traveled to the LUMO level of ETL and hole went to the HOMO level of HTL. Therefore, it was important to install each layer sequentially and moderately to extract the charge carrier with minimizing the energy loss. But in our device and energy level diagram, there was an unsuitable energy level between HTL and Au. So, there were some disadvantages as we assembled the device structure. In the figure, the LUMO metal oxide energy level showed lower value than that of HTL, meaning that hole carrier might be disturbed

ULSAN NATIONAL INSTITUTE OF SCIENCE AND TECHNOLOGY

to move to the electrode side, as the metal oxide was naturally used for electron transport. Therefore, the metal oxide layers might play a role as a hole blocking barrier. In the J-V curve of opaque cells, device containing metal oxide interlayer had decreased V_{oc} by this reason.

Also, we fabricated opaque perovskite cell with MoO_x interlayer between HTL and Au electrode. In Figure 12, device performance of initial time did not show prominent differences. But after 24 hours from first measurement, the parameters of device performance were stiffly degraded. We suggested that the rapid degradation of opaque solar cell performance with MoO_x interlayer was due to the interface problem. In the case of MoO_x/Al electrode, Al metal reacted with MoO_x film to format Al_2O_3. And the Al_2O_3 film made by the reaction was an additional interlayer to improve stability of device by blocking the moisture. MoO_x was a hydroscopic material so it had a property to drain the moisture from the room atmosphere humidity. Perovskite material was soluble to water, so if MoO_x layer drained humidity from air, the performance of perovskite device could be dramatically damaged. So, the Al_2O_3 interlayer from Al electrode could be proper barrier from the degradation. But with the Au or Ag electrode, MoO_x did not react with Au and Ag electrode, so the underlayers could be easily exposed to the humidity from air. As a result, although the initial performances were good comparing with Al electrode, MoO_x quickly degraded the performances just after few hours.

ULSAN NATIONAL INSTITUTE OF SCIENCE AND TECHNOLOGY

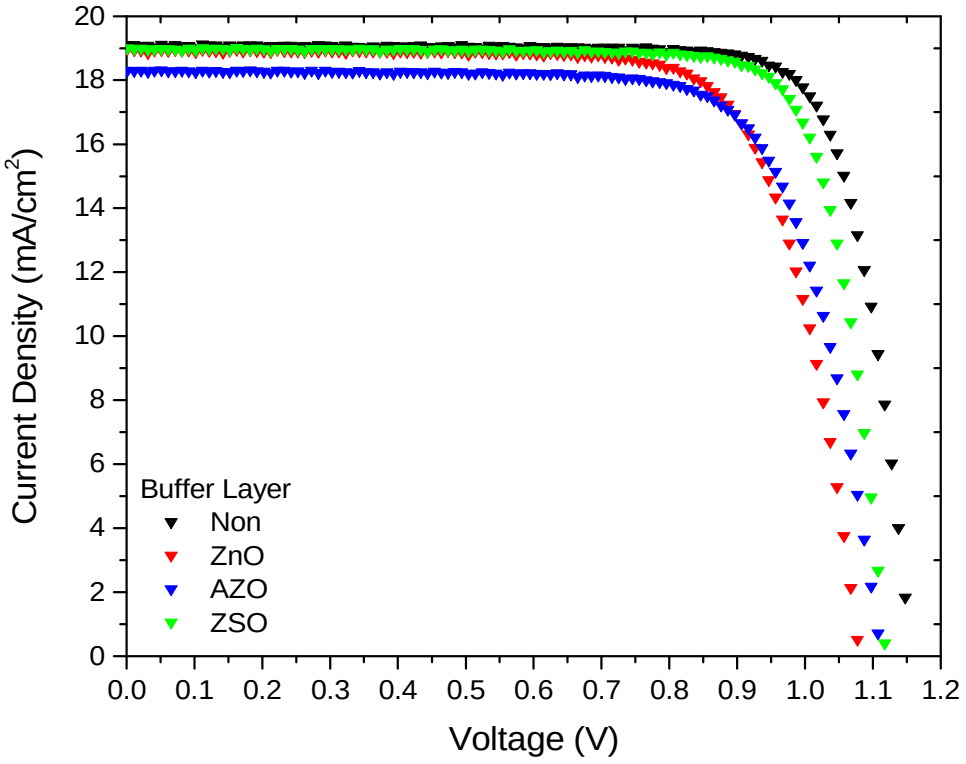

Figure 11. J-V characteristic of opaque device with varied buffer layer.

Table 1. Performances of opaque solar cell in Figure 11.

	J_{sc}(mA/cm2)	V_{oc}(V)	FF (%)	Eff. (%)
Non	19.1	1.16	80.4	17.79
ZnO	19.0	1.08	74.9	15.31
AZO	18.3	1.11	74.8	15.18
ZTO	19.0	1.12	80.7	17.15

ULSAN NATIONAL INSTITUTE OF SCIENCE AND TECHNOLOGY

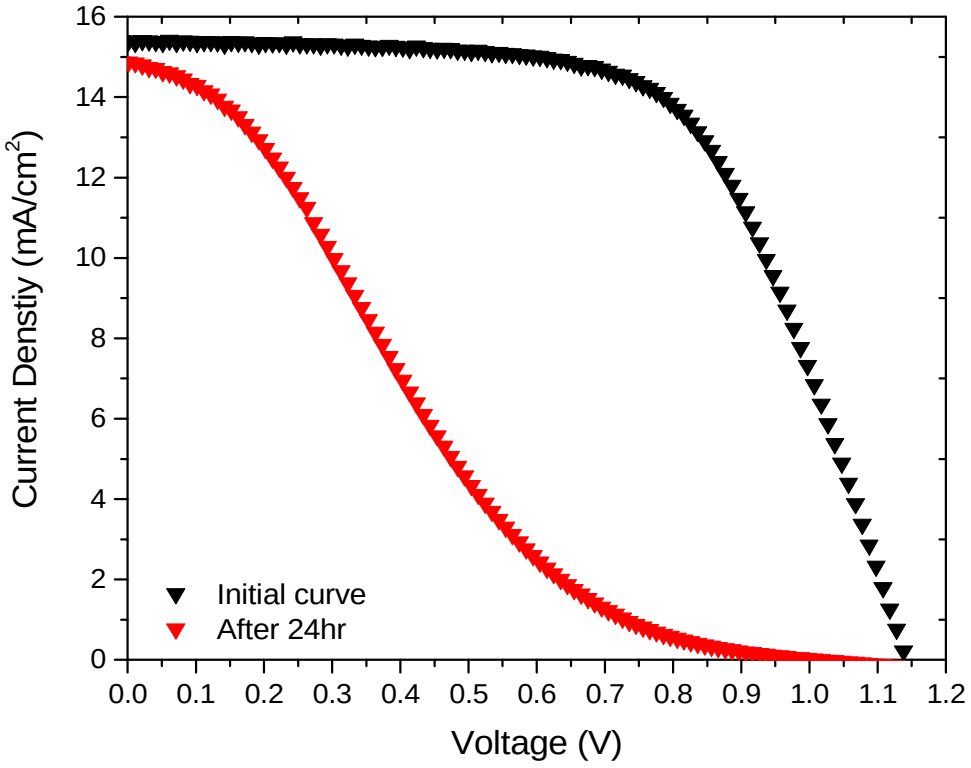

Figure 12. J-V characteristic of solar cell with molybdenum oxide and Au electrode over time.

Table 2. Photovoltaic performances of opaque solar cell in Figure 12.

	Jsc(mA/cm^2)	Voc(V)	FF	Eff.(%)
Initial Performance	15.4	1.14	63.1	11.06
After 24hr	14.9	1.02	20	3.03

ULSAN NATIONAL INSTITUTE OF SCIENCE AND TECHNOLOGY

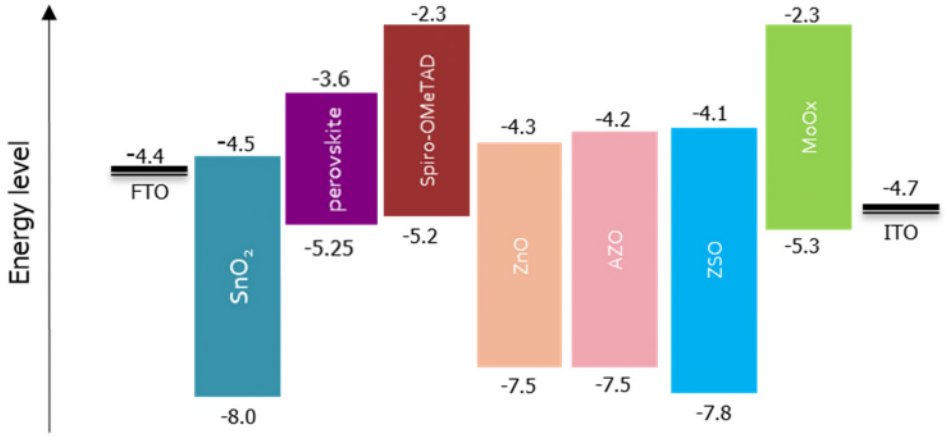

Figure 13. Schematic energy diagram of semi-transparent solar cell

To check the coverage of Zn_2SnO_4 as it was coated by solution process, we measured the surface images of ZTO nanoparticles and ZTO/MoO_x layer on spiro-OMeTAD. In the images of surface, we could see the agglomerated ZTO nanoparticles on HTL. The ZTO nanoparticles on HTL showed the uneven surface coverage. It was thought that the difference of the disperse solvent of ZTO nanoparticles affected to the surface morphology. The particle size of Zn_2SnO_4 was measured by normal TEM. Figure 15 showed the TEM image of Zn_2SnO_4 nanoparticles. The dispersed Zn_2SnO_4 were diluted with isopropanol and dropped on copper grid. The average size of Zn_2SnO_4 particle was 5~10nm.

Figure 16 shows XRD characterization of Zn_2SnO_4 nanoparticles. The pattern of XRD showed the crystal formation of Zn_2SnO_4 as a face centered cubic structure. The pattern illustrated that the synthesize of Zn_2SnO_4 by hydrothermal process resulted well as it closely matched with stoichiometric ratio.

ULSAN NATIONAL INSTITUTE OF SCIENCE AND TECHNOLOGY

a.

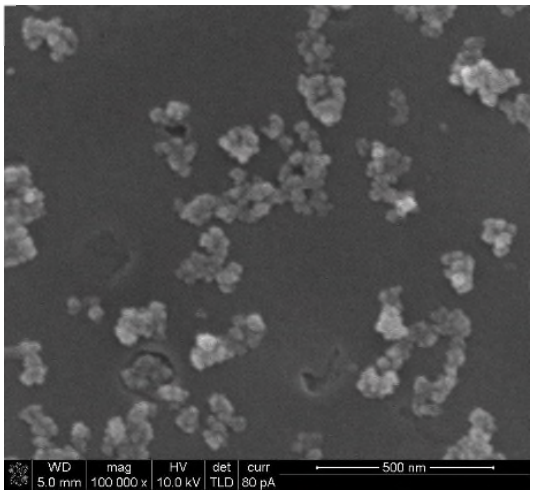

b.

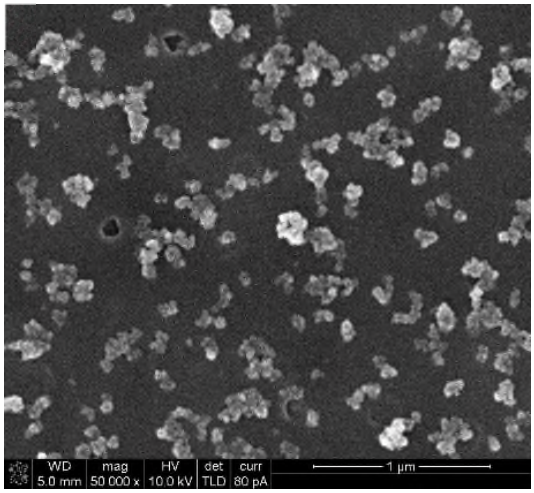

Figure 14. SEM image of Spiro-OMeTAD surface with (a) Zn2SnO4 nanoparticles and (b) ZTO/MoO_x buffer layer

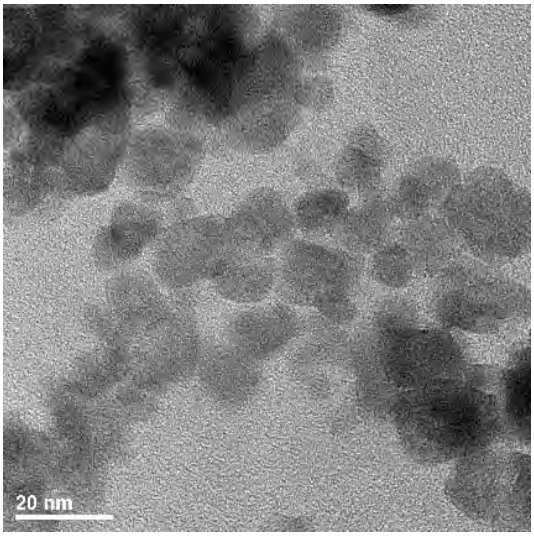

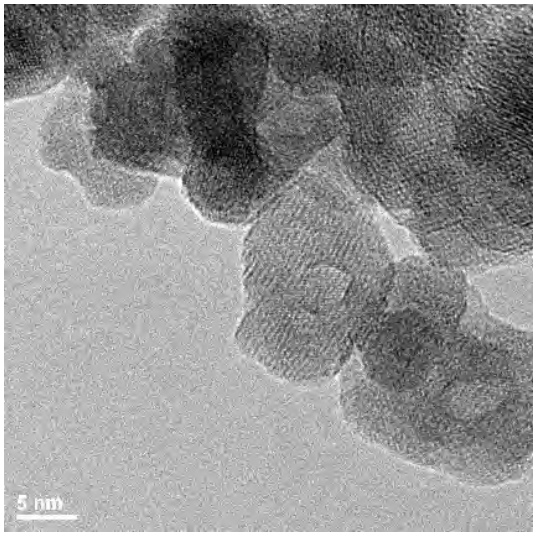

Figure 15. TEM images of Zn_2SnO_4 nanoparticles.

ULSAN NATIONAL INSTITUTE OF SCIENCE AND TECHNOLOGY

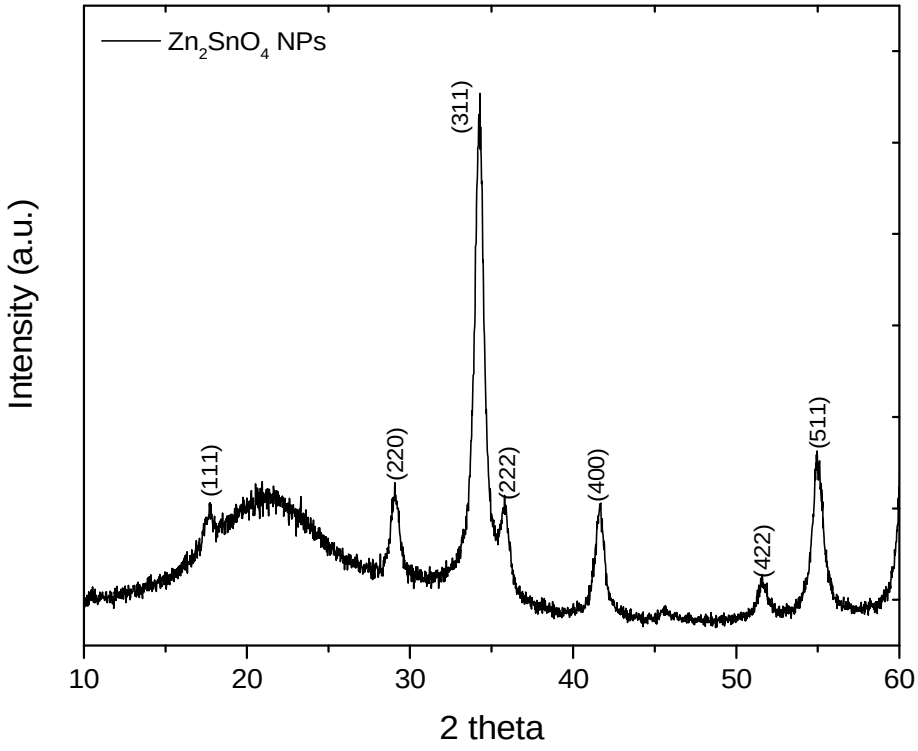

Figure 16. X-ray diffraction patterns of Zn_2SnO_4 nanoparticles.

ULSAN NATIONAL INSTITUTE OF SCIENCE AND TECHNOLOGY

Then we checked the SEM cross image with different buffer layer conditions. Firstly, we checked the surface morphology of sputtered ITO. And then we compared the films of perovskite and spiro-OMeTAD with ITO sputter by each buffer layer condition. Figure b. showed the image of sputtered ITO directly on HTL without any buffer layers. In perovskite layer, there were no distinct evidences of the plasma damage during ITO sputtering progress. But in the HTL, there were some hollow defects found in the spiro-OMeTAD layer. Also, in figure c, which contained MoOx buffer layer between HTL and ITO, there were any hollow defects in the hole transport layer. We assumed that these hole defects were related to the degradation by plasma damage. Then we checked the feasibility of ZTO nanoparticles whether they could block the sputtering damage or not. The result showed that single ZTO layer could not reduce the sputtering damage. It showed that the HTL of figure d also had hollow defects in the layer.

To find the detail effects of buffer layer to perovskite, we divided and compared x-ray diffraction peaks of perovskite film with varied condition. We set the reference peak (black line) with the pristine perovskite film. Then we measured each semi-transparent solar cell with ITO and different buffer layers. In the data, there were no different peaks of perovskite with the reference condition. All ZTO, MoO_x, and ZTO/MoO_x conditions showed the same location of peaks which meant the ITO sputtering process with different buffer layer condition did not affect to the perovskite structure.

ULSAN NATIONAL INSTITUTE OF SCIENCE AND TECHNOLOGY

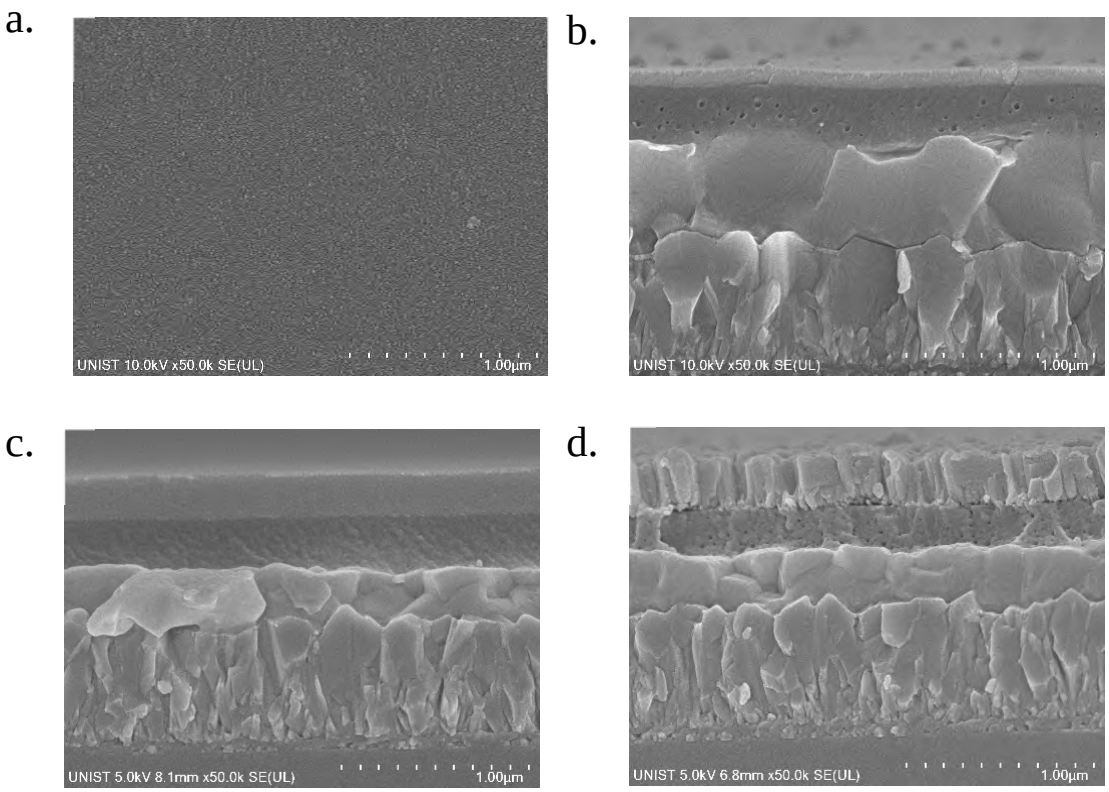

Figure 17. SEM images of semi-transparent solar cells. (a) surface image of ITO sputtered cell. (b) Cross image of semi-transparent solar cell without any buffer layer. (c) semi-transparent solar cell with MoO_x buffer layer. (d) semi-transparent solar cell with ZTO nanoparticles between HTL and ITO electrode.

ULSAN NATIONAL INSTITUTE OF SCIENCE AND TECHNOLOGY

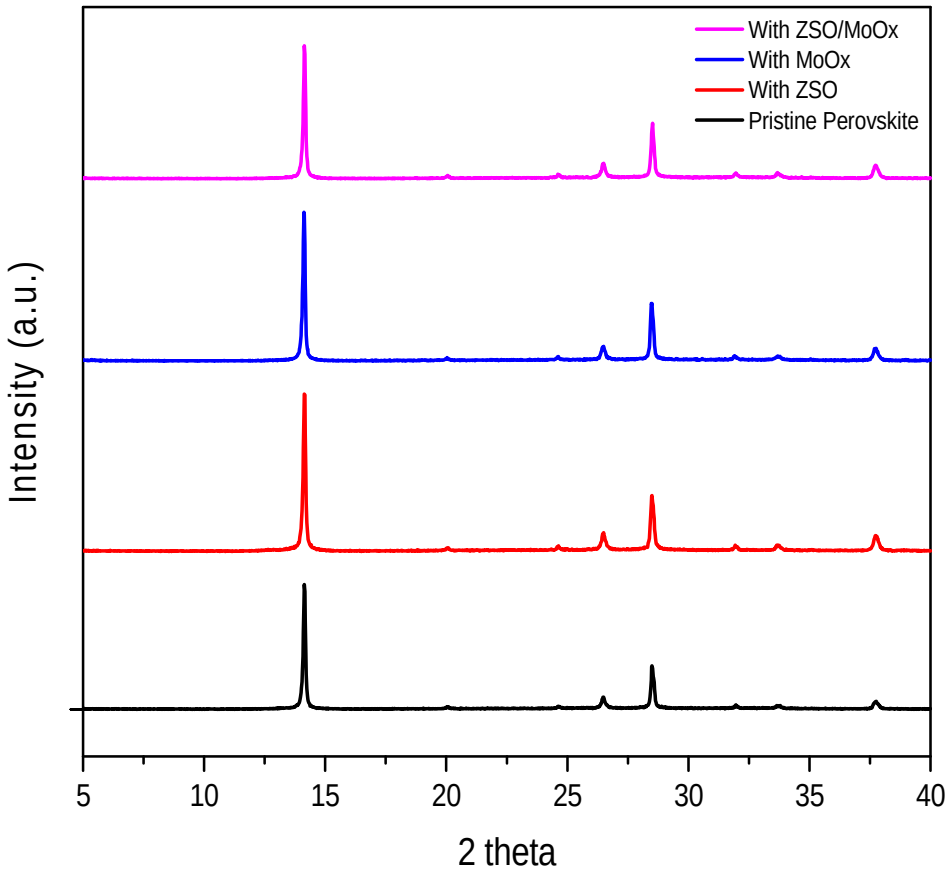

Figure 18. X-ray diffraction patterns of pristine perovskite film and perovskites with varied buffer layer and ITO electrode.

ULSAN NATIONAL INSTITUTE OF SCIENCE AND TECHNOLOGY

3.2 Device performance with combined buffer layer

We checked the absorbance of perovskite film by different ratio of $FAPbI_3$ and $MAPbBr_3$. In the figure, we fabricated 4 kinds of perovskite with varied ratio. It resulted blue-shifted band gaps by increasing amounts of $MAPbBr_3$, which contained bromine to increase the band gap energy.

For the metal oxide nanoparticle buffer layer, we compared the semi-transparent perovskite solar cell conversion efficiency with ZnO, AZO, ZTO nanoparticles. MoO_x layer was additionally evaporated. In the figure, all those perovskite cell with ITO electrode showed similar efficiency, but the perovskite cell with ZTO nanoparticles showed higher current density rather and other conditions.

To measure the effects of nanoparticles to absorbance, we checked the transmittance spectra of MoO_x layer and other buffer layer conditions with ITO. Both ITO conditions with MoOx buffer layer showed 75% average transmittance from 300 to 1300 nm of wavelengths. We thought that the ZTO nanoparticles did not affect to the transmittance of perovskite solar cell. Rather, MoO_x layer affected to the transmittance because the ZTO/ITO layer showed 7% higher transmittance rather than other two conditions. Then, we checked the transmittance of full device of semi-transparent solar cell. In the full device, the average transmittance in the range of over 800nm of wavelength showed over 70%. It showed that semi-transparent solar cell was enough to send near infrared spectrum to the rear subcell.

To check the conversion efficiency of different semi-transparent perovskite cells, we constructed perovskite solar cells in different buffer layer conditions. Figure 22 showed the J-V data and its efficiency of semi-transparent solar cells with 1.0 cm^2 of active area. Without any buffer layer for ITO sputtering process, perovskite cell showed S-shape of its curve with degraded fill factor and efficiency. And with the MoO_x buffer layer, the perovskite cell showed higher V_{oc} and enhanced efficiency. The efficiency of perovskite cell furtherly increased when the ZTO nanoparticles were added before MoO_x evaporation. These phenomena were also found in the small active area (0.094 cm^2) of perovskite solar cells. In the figure 23, ZTO/MoO_x buffer layer condition showed the highest efficiency rather than others. The external quantum efficiency (EQE) and steady state of semi-transparent device with ZTO/MoO_x buffer layer was measured. Both data showed the current density about 16.8 ~ 17 mA/cm2. And we found a decrease of the absorption of longer wavelength in a EQE spectrum. The best performance of semi-transparent solar cell with ZTO/MoO_x buffer layer was shown in figure. It showed 15.61% of its efficiency with 17.99 mA/cm^2 of current density, 1.13 V of V_{oc}, and 77.11% of fill factor.

ULSAN NATIONAL INSTITUTE OF SCIENCE AND TECHNOLOGY

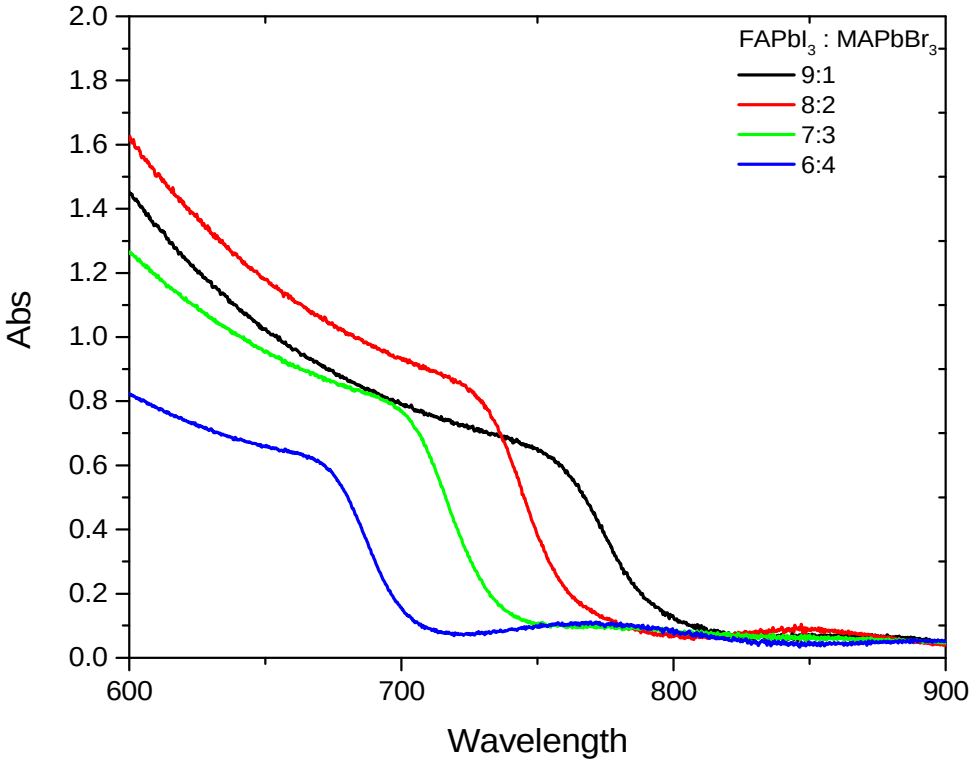

Figure 19. UV-vis absorption with different halide anion and organic cation ratio of perovskite

ULSAN NATIONAL INSTITUTE OF
SCIENCE AND TECHNOLOGY

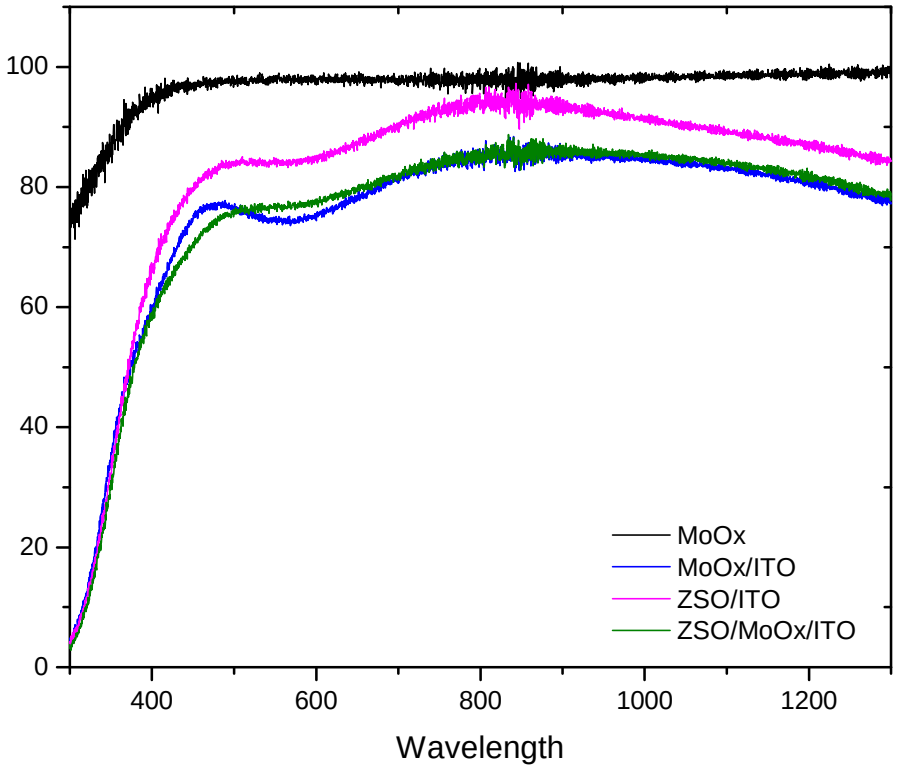

Figure 20. Transmittance spectra of MoO_x buffer layer and sputtered ITO with varied buffer layer conditions.

ULSAN NATIONAL INSTITUTE OF SCIENCE AND TECHNOLOGY

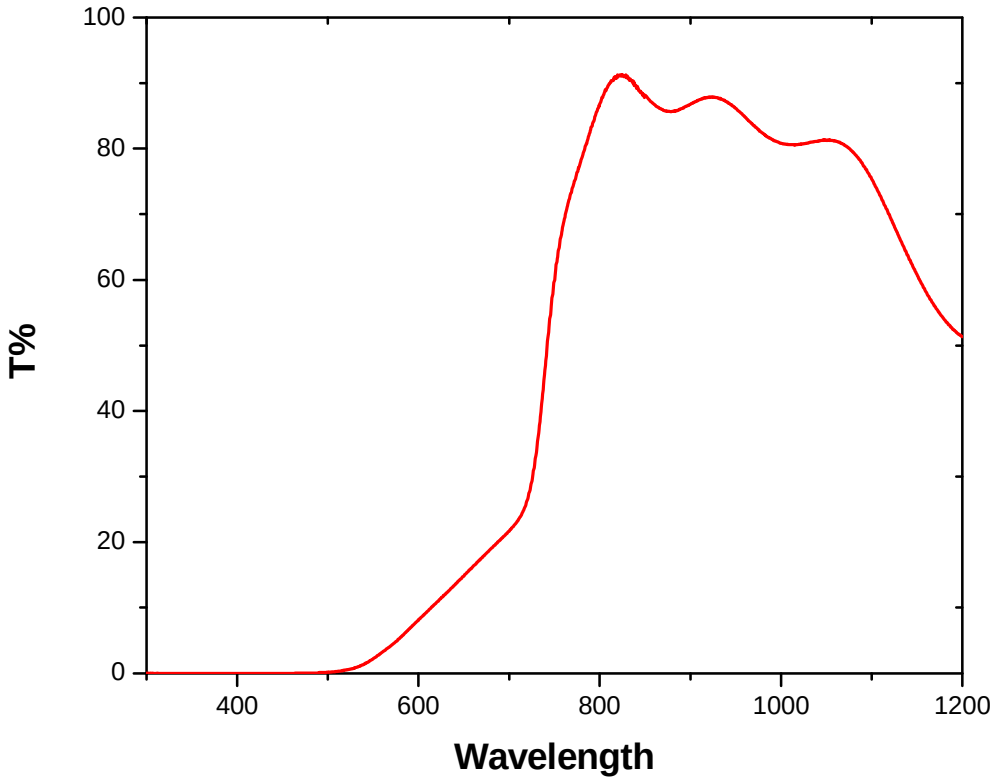

Figure 21. Transmittance spectra of semi-transparent solar cell with ZTO/MoO_x buffer layer

ULSAN NATIONAL INSTITUTE OF SCIENCE AND TECHNOLOGY

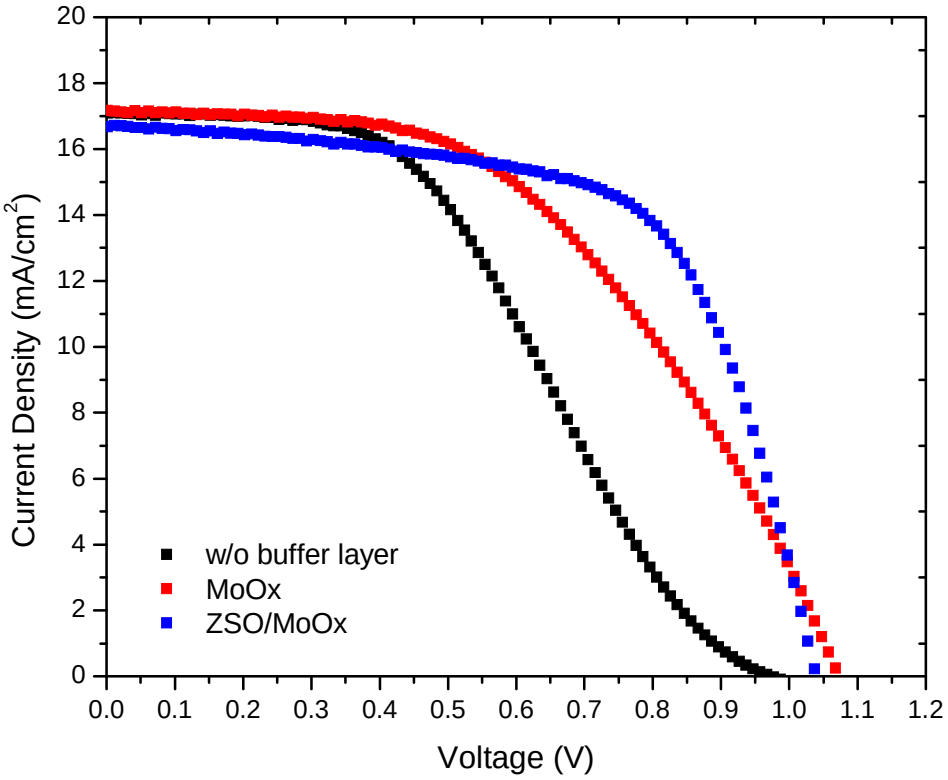

Figure 22. J-V characteristics of semi-transparent devices with varied buffer layer conditions measured with a large active area (1.00 cm^2)

Table 3. Photovoltaic performances of semi-transparent devices in Figure 22.

	Jsc(mA/cm2)	Voc(V)	FF	Eff.(%)
w/o buffer layer	17.1	0.98	42.8	7.14
MoOx	17.2	1.07	49.7	9.12
ZTO/MoOx	16.7	1.04	63.8	11.04

ULSAN NATIONAL INSTITUTE OF SCIENCE AND TECHNOLOGY

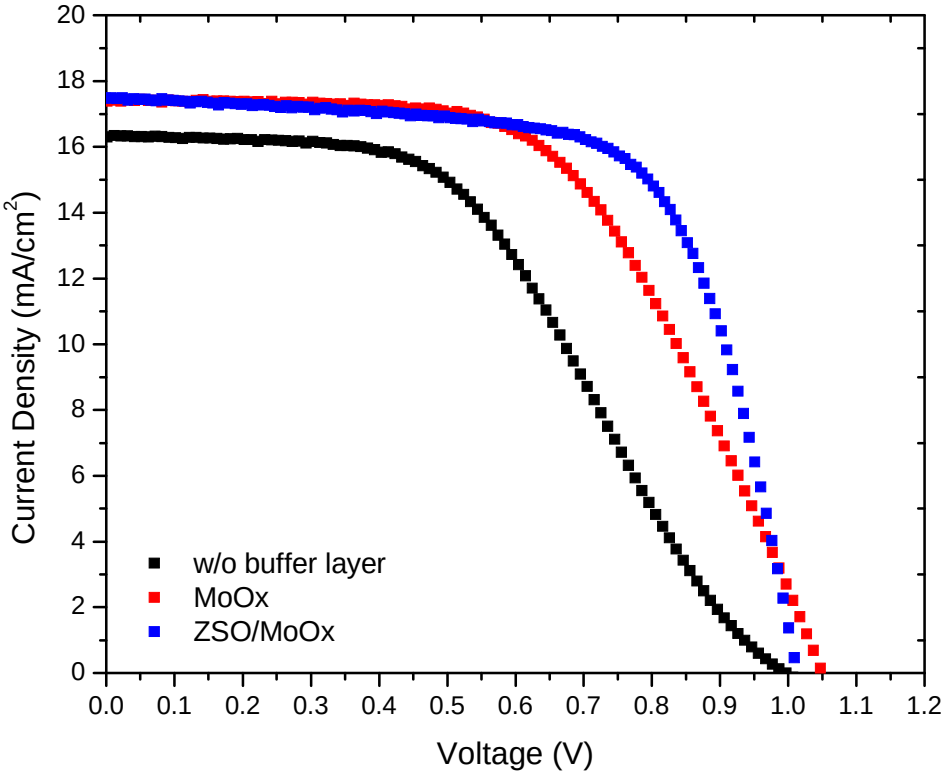

Figure 23. J-V characteristics of semi-transparent solar cell with varied buffer layer conditions measured with a small active area (0.094 cm^2)

Table 4. Photovoltaic performances of semi-transparent solar cells in Figure 23.

	Jsc(mA/cm2)	Voc(V)	FF	Eff.(%)
w/o buffer layer	16.3	1.00	47.3	7.69
MoOx	17.4	1.05	56.9	10.37
ZTO/MoOx	17.5	1.01	67.8	11.96

ULSAN NATIONAL INSTITUTE OF SCIENCE AND TECHNOLOGY

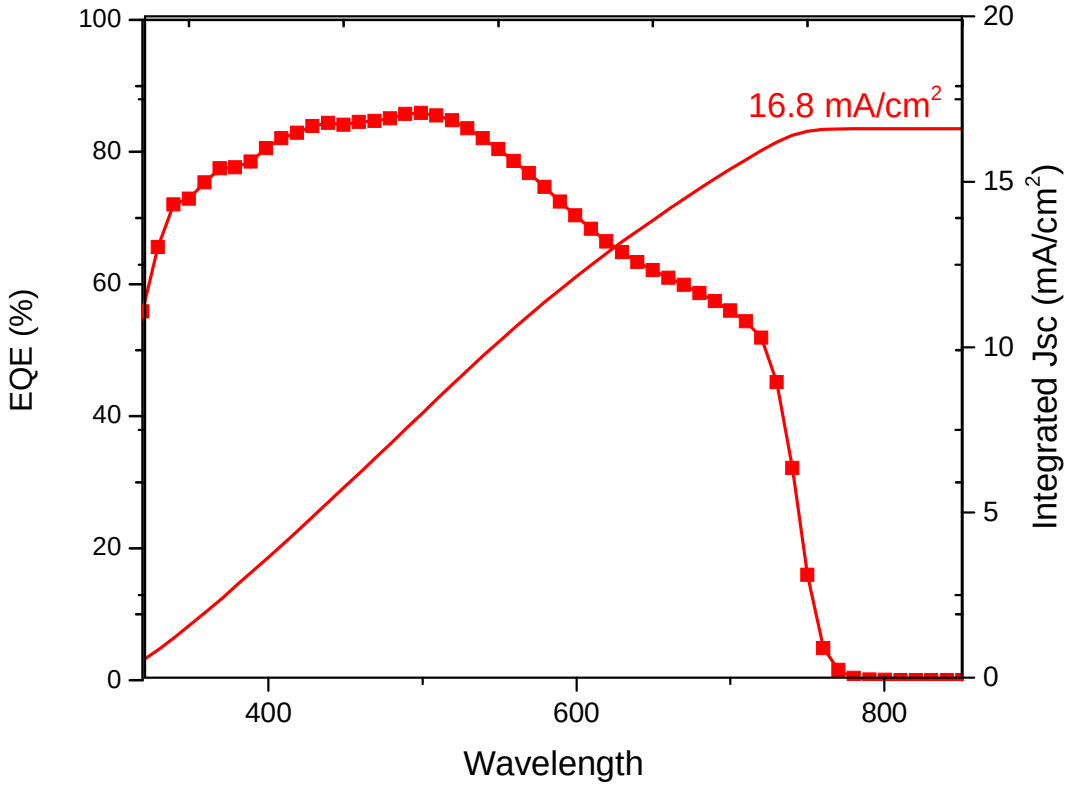

Figure 21. EQE spectra of semi-transparent solar cell with ZTO/MoO_x buffer layer

ULSAN NATIONAL INSTITUTE OF
SCIENCE AND TECHNOLOGY

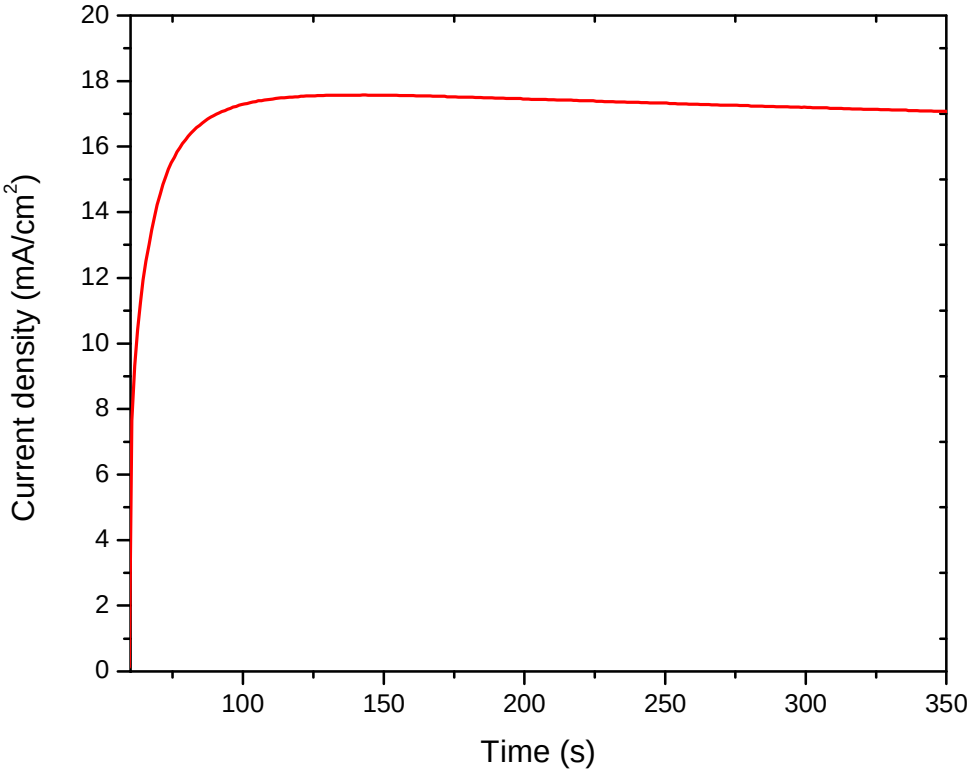

Figure 22. Steady state of semi-transparent perovskite solar cell with ZTO/MoO_x buffer layer

ULSAN NATIONAL INSTITUTE OF SCIENCE AND TECHNOLOGY

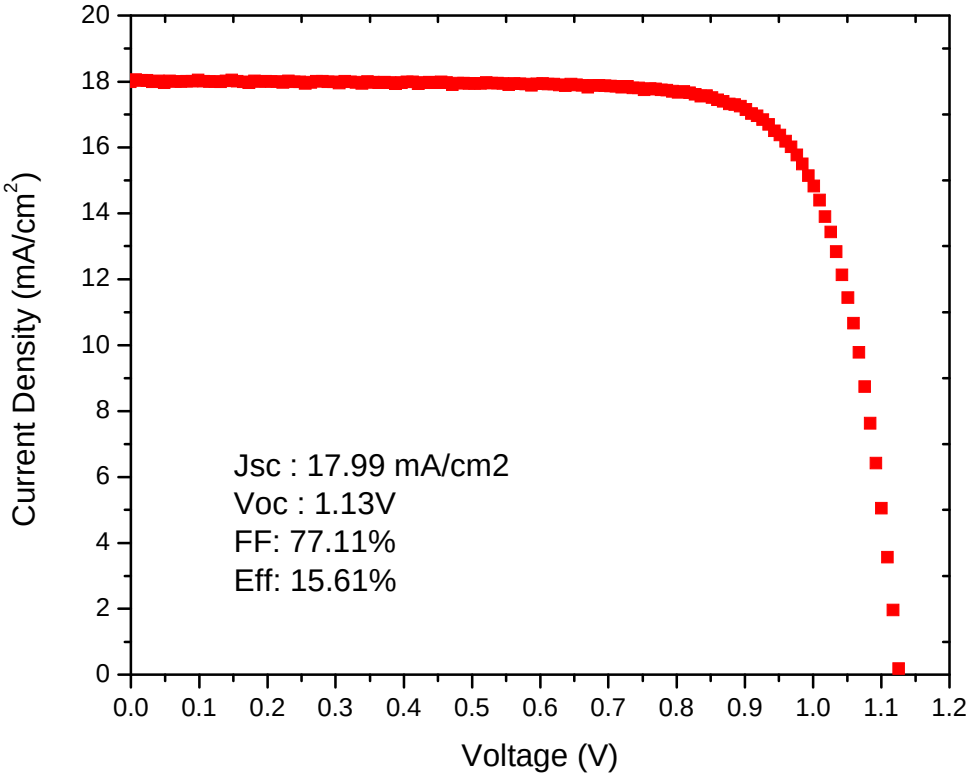

Figure 23. J-V characteristic of best semi-transparent perovskite device. Atmosphere condition of fabrication was ambient condition. (25 ℃, humidity 25 %)

The stability of semitransparent with each buffer layer condition was also checked in different storage conditions. In a room temperature storage, ZTO single coated perovskite cell showed good stability after 900 hours. But the efficiency of the cell was low, around 6% of its initial efficiency. MoO_x coated solar cell showed higher initial efficiency than ZTO single coated solar cell, recording over 11%. But the efficiency in ambient condition was gradually decreased, reaching almost 0% after 900hours. But with the combined buffer layer, the stability of solar cell did not much decreased, maintaining almost 70% of its initial efficiency after 900 hours. These phenomena were also shown in the 85℃ thermal storage condition. With the MoO_x layer, the efficiency dramatically decreased just after few hours. This degradation also happened in the ZTO/MoO_x condition in the beginning. But after enough time, the efficiency maintained its stability over 60% of initial value.

ULSAN NATIONAL INSTITUTE OF SCIENCE AND TECHNOLOGY

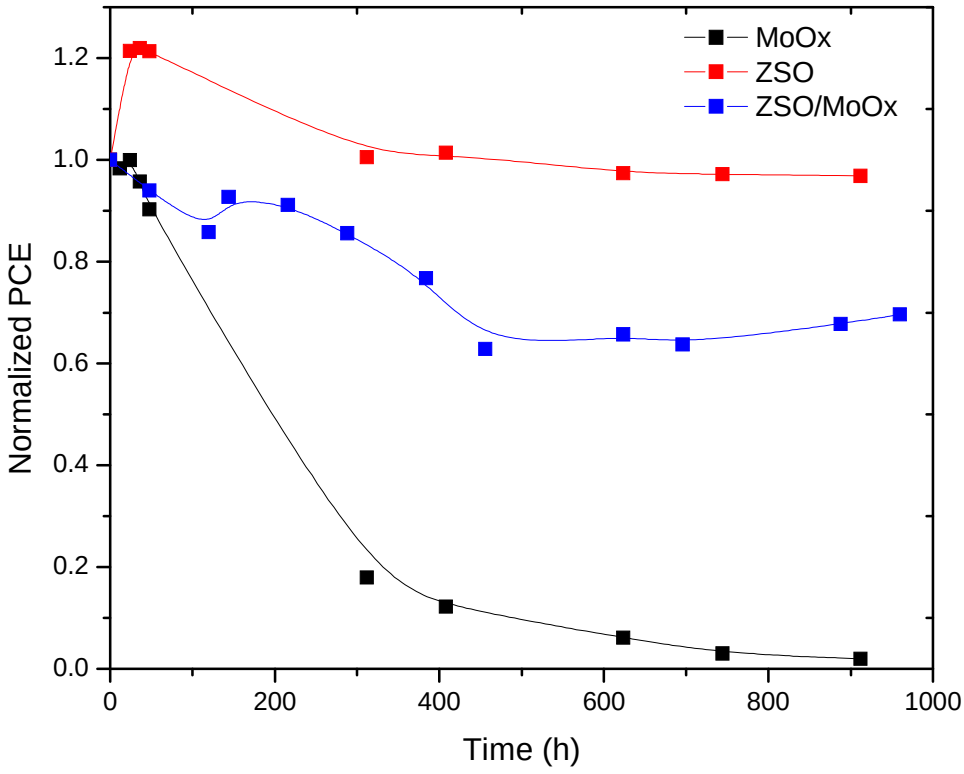

Figure 24. Stability test of semi-transparent perovskite solar cell efficiencies in ambient room condition

ULSAN NATIONAL INSTITUTE OF SCIENCE AND TECHNOLOGY

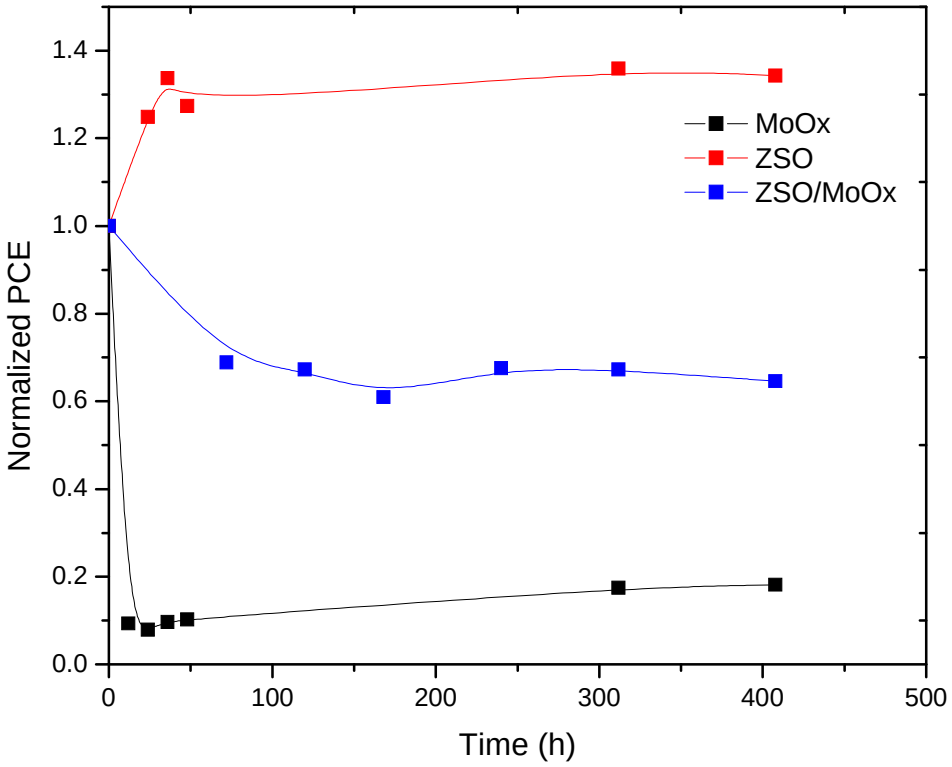

Figure 25. Stability test of semi-transparent perovskite solar cell efficiencies in 85℃ thermal condition

ULSAN NATIONAL INSTITUTE OF SCIENCE AND TECHNOLOGY

IV. Conclusion

From the emergence of perovskite solar cell in 2009, photovoltaic performances of perovskite solar cell were highly accelerated from less than 5% to 24.2% in a short time. Additionally, perovskite materials were applied to multijunction structure of solar cells, including tandem to overcome to the efficiency limitation (Shockley-Queisser limits) of single junction. To fabricate multijunction solar cell, transparent conducting oxide layer was necessary to transmit a sunlight to rear junction of solar cell. And during the sputtering process of TCOs by magnetron sputtering method, it was found that the organic layers of perovskite solar cell were exposed to plasma environments which degraded performance of solar cells. In n-i-p structure, MoO_x showed outstanding ability of blocking this plasma damage for organic charge transfer layer. But in the stability issues, MoO_x itself had a hygroscopic property which induced moisture passing problem. Also, there was found an interface problem between MoO_x and solar cell electrode, so the efficiency desperately degraded just after few hours. We tried to take the stability issue of semi-transparent solar cell by combining MoO_x and ZTO metal oxide nanoparticles. Although it was not clear exactly what happened in the interfaces between MoO_x and ZTO, the semi-transparent perovskite solar cell showed much improved stability both in ambient and thermal conditions. We expected that by studying the interface effects with MoO_x and these nanoparticles, the stability of solar cells with MoO_x buffer layer could be advanced.

ULSAN NATIONAL INSTITUTE OF SCIENCE AND TECHNOLOGY

References

1. Shi, D., Adinolfi, V., Comin, R., Yuan, M., Alarousu, E., Buin, A., . . . Bakr, O. M. (2015). Low trap-state density and long carrier diffusion in organolead trihalide perovskite single crystals. Science, 347(6221), 519-522

2. Kojima, A., Teshima, K., Miyasaka, T. & Shirai, Y. Novel photoelectrochemical cell with mesoscopic electrodes sensitized by lead-halide compounds (2). in Proc. 210th ECS Meeting (ECS, 2006).

3. Kojima, A., Teshima, K., Shirai, Y., & Miyasaka, T. (2009). Organometal Halide Perovskites as Visible-Light Sensitizers for Photovoltaic Cells. Journal of the American Chemical Society, 131(17), 6050-6051

4. Im, J., Lee, C., Lee, J., Park, S., & Park, N. (2011). 6.5% efficient perovskite quantum-dot-sensitized solar cell. Nanoscale, 3(10), 4088

5. Kim, H., Lee, C., Im, J., Lee, K., Moehl, T., Marchioro, A., . . . Park, N. (2012). Lead Iodide Perovskite Sensitized All-Solid-State Submicron Thin Film Mesoscopic Solar Cell with Efficiency Exceeding 9%. Scientific Reports, 2(1).

6. Lee, M. M., Teuscher, J., Miyasaka, T., Murakami, T. N. & Snaith, H. J. Efficient hybrid solar cells based on meso-superstructured organometal halide perovskites. Science 338, 643–647 (2012).

7. Noh, J. H., Im, S. H., Heo, J. H., Mandal, T. N., & Seok, S. I. (2013). Chemical Management for Colorful, Efficient, and Stable Inorganic–Organic Hybrid Nanostructured Solar Cells. Nano Letters, 13(4), 1764-1769

8. Jeon, N. J., Noh, J. H., Kim, Y. C., Yang, W. S., Ryu, S., & Seok, S. I. (2014). Solvent engineering for high-performance inorganic–organic hybrid perovskite solar cells. Nature Materials, 13(9), 897-903

9. Yang, W. S., Noh, J. H., Jeon, N. J., Kim, Y. C., Ryu, S., Seo, J., & Seok, S. I. (2015). High-performance photovoltaic perovskite layers fabricated through intramolecular exchange. Science, 348(6240), 1234-1237

10. Jeon, N. J., Noh, J. H., Yang, W. S., Kim, Y. C., Ryu, S., Seo, J., & Seok, S. I. (2015). Compositional engineering of perovskite materials for high-performance solar cells. Nature, 517(7535), 476-480

11. Yun, J. S., Seidel, J., Kim, J., Soufiani, A. M., Huang, S., Lau, J., . . . Ho-Baillie, A. (2016). Critical Role of Grain Boundaries for Ion Migration in Formamidinium and Methylammonium Lead Halide Perovskite Solar Cells. Advanced Energy Materials, 6(13), 1600330

12. Kim, Y. C., Jeon, N. J., Noh, J. H., Yang, W. S., Seo, J., Yun, J. S., Ho-Baillie, A., Huang, S., Green, M. A., Seidel, J., Ahn, T. K., Seok, S. I. (2016). Beneficial Effects of PbI_2 Incorporated in Organo-Lead Halide Perovskite Solar Cells. Adv. Energy Mater., 6: 1502104.

13. Yang, W. S., Park, B., Jung, E. H., Jeon, N. J., Kim, Y. C., Lee, D. U., . . . Seok, S. I. (2017). Iodide management in formamidinium-lead-halide–based perovskite layers for efficient solar cells. Science, 356(6345), 1376-1379

14. Park, B., Kedem, N., Kulbak, M., Lee, D. Y., Yang, W. S., Jeon, N. J., . . . Seok, S. I. (2018). Understanding how excess lead iodide precursor improves halide perovskite solar cell performance. Nature Communications, 9(1).

ULSAN NATIONAL INSTITUTE OF SCIENCE AND TECHNOLOGY

15. Jeon, N. J., Na, H., Jung, E. H., Yang, T., Lee, Y. G., Kim, G., . . . Seo, J. (2018). A fluorene-terminated hole-transporting material for highly efficient and stable perovskite solar cells. Nature Energy, 3(8), 682-689

16. https://www.nrel.gov/pv/assets/pdfs/pv-efficiency-chart.20190416

17. Yaoguang R., Yue Hu, Anyi Mei, Hairen Tan (2018). Challenges for commercializing perovskite solar cells. Science, 361, 6408

18. Taame Abraha Berhe, Wei-Nien Su, Ching-Hsiang Chen, Chun-Jern Pan. Organometal halide perovskite solar cells: degradation and stability. Energy Environ. Sci., 2016, 9, 323—356

19. A. M. A. Leguy, Y. Hu, M. Campoy-Quiles, M. I. Alonso, O. J. Weber, P. Azarhoosh, M. van Schilfgaarde, M. T. Weller, T. Bein, J. Nelson, P. Docampo and P. R. F. Barnes, Chem. Mater., 2015, 27, 3397–3407

20. You, J., Meng, L., Song, T., Guo, T., Yang, Y., Chang, W., . . . Yang, Y. (2015). Improved air stability of perovskite solar cells via solution-processed metal oxide transport layers. Nature Nanotechnology, 11(1), 75-81

21. Z. Wang, Z. Shi, T. Li, Y. Chen and W. Huang, Stability of Perovskite Solar Cells: A Prospective on the Substitution of the A Cation and X Anion. Angew. Chem., Int. Ed., 2016, 56, 1190–1212

22. Saliba, M., Matsui, T., Seo, J., Domanski, K., Correa-Baena, J., Nazeeruddin, M. K., . . . Grätzel, M. (2016). Cesium-containing triple cation perovskite solar cells: Improved stability, reproducibility and high efficiency. Energy & Environmental Science, 9(6), 1989-1997

23. Kulbak, M., Gupta, S., Kedem, N., Levine, I., Bendikov, T., Hodes, G., & Cahen, D. (2015). Cesium Enhances Long-Term Stability of Lead Bromide Perovskite-Based Solar Cells. The Journal of Physical Chemistry Letters, 7(1), 167-172

24. Li, W., Zhang, W., Reenen, S. V., Sutton, R. J., Fan, J., Haghighirad, A. A., . . . Snaith, H. J. (2016). Enhanced UV-light stability of planar heterojunction perovskite solar cells with caesium bromide interface modification. Energy & Environmental Science, 9(2), 490-498

25. Min, H., Kim, G., Paik, M. J., Lee, S., Yang, W. S., Jung, M., & Seok, S. I. (2019). Perovskite Solar Cells: Stabilization of Precursor Solution and Perovskite Layer by Addition of Sulfur (Adv. Energy Mater. 17/2019). Advanced Energy Materials, 9(17), 1970056

26. Smith, I. C., Hoke, E. T., Solis-Ibarra, D., Mcgehee, M. D., & Karunadasa, H. I. (2014). A Layered Hybrid Perovskite Solar-Cell Absorber with Enhanced Moisture Stability. Angewandte Chemie, 126(42), 11414-11417

27. Quan, L. N., Yuan, M., Comin, R., Voznyy, O., Beauregard, E. M., Hoogland, S., . . . Sargent, E. H. (2016). Ligand-Stabilized Reduced-Dimensionality Perovskites. Journal of the American Chemical Society, 138(8), 2649-2655

28. Tsai, H., Nie, W., Blancon, J., Stoumpos, C. C., Asadpour, R., Harutyunyan, B., . . . Mohite, A. D. (2016). High-efficiency two-dimensional Ruddlesden–Popper perovskite solar cells. Nature, 536

29. Löper, P., Moon, S., Nicolas, S. M., Niesen, B., Ledinsky, M., Nicolay, S., . . . Ballif, C. (2015). Organic–inorganic halide perovskite/crystalline silicon four-terminal tandem solar cells. Physical Chemistry Chemical Physics, 17(3), 1619-1629

30. Werner, J., Dubuis, G., Walter, A., Löper, P., Moon, S., Nicolay, S., . . . Ballif, C. (2015). Sputtered rear electrode with broadband transparency for perovskite solar cells. Solar Energy Materials and

ULSAN NATIONAL INSTITUTE OF SCIENCE AND TECHNOLOGY

Solar Cells, 141, 407-413

31. Duong, T., Lal, N., Grant, D., Jacobs, D., Zheng, P., Rahman, S., . . . Catchpole, K. R. (2016). Semitransparent Perovskite Solar Cell With Sputtered Front and Rear Electrodes for a Four-Terminal Tandem. IEEE Journal of Photovoltaics, 6(3), 679-687

32. Chen, B., Bai, Y., Yu, Z., Li, T., Zheng, X., Dong, Q., . . . Huang, J. (2016). Efficient Semitransparent Perovskite Solar Cells for 23.0%-Efficiency Perovskite/Silicon Four-Terminal Tandem Cells. Advanced Energy Materials, 6(19), 1601128

33. Werner, J., Barraud, L., Walter, A., Bräuninger, M., Sahli, F., Sacchetto, D., . . . Ballif, C. (2016). Efficient Near-Infrared-Transparent Perovskite Solar Cells Enabling Direct Comparison of 4-Terminal and Monolithic Perovskite/Silicon Tandem Cells. ACS Energy Letters, 1(2), 474-480

34. Peng, J., Duong, T., Zhou, X., Shen, H., Wu, Y., Mulmudi, H. K., . . . White, T. P. (2016). Efficient Indium-Doped TiO_x Electron Transport Layers for High-Performance Perovskite Solar Cells and Perovskite-Silicon Tandems. Advanced Energy Materials, 7(4), 1601768

35. Duong, T., Wu, Y., Shen, H., Peng, J., Fu, X., Jacobs, D., . . . Catchpole, K. (2017). Rubidium Multication Perovskite with Optimized Bandgap for Perovskite-Silicon Tandem with over 26% Efficiency. Advanced Energy Materials, 7(14), 1700228

36. Mailoa, J. P., Bailie, C. D., Johlin, E. C., Hoke, E. T., Akey, A. J., Nguyen, W. H., . . . Buonassisi, T. (2015). A 2-terminal perovskite/silicon multijunction solar cell enabled by a silicon tunnel junction. Applied Physics Letters, 106(12), 121105

37. Werner, J., Weng, C., Walter, A., Fesquet, L., Seif, J. P., Wolf, S. D., . . . Ballif, C. (2015). Efficient Monolithic Perovskite/Silicon Tandem Solar Cell with Cell Area 1 cm^2. The Journal of Physical Chemistry Letters, 7(1), 161-166

38. Bush, K. A., Palmstrom, A. F., Yu, Z. J., Boccard, M., Cheacharoen, R., Mailoa, J. P., . . . Mcgehee, M. D. (2017). 23.6%-efficient monolithic perovskite/silicon tandem solar cells with improved stability. Nature Energy, 2(4).

39. Giles E. Eperon, Tomas L., & Henry J. Snaith (2016) Perovskite-perovskite tandem photovoltaics with optimized band gaps, Science, 354, 6314

40. Borriello, I., Cantele, G., & Ninno, D. (2008). Ab initio investigation of hybrid organic-inorganic perovskites based on tin halides. Physical Review B, 77(23)

41. Rajagopal, A., Yang, Z., Jo, S. B., Braly, I. L., Liang, P., Hillhouse, H. W., & Jen, A. K. (2017). Highly Efficient Perovskite-Perovskite Tandem Solar Cells Reaching 80% of the Theoretical Limit in Photovoltage. Advanced Materials, 29(34), 1702140

42. David F., Lidon G., Daniel P., Cristina M., Jeremie W., . . . Henk J. Bolink (2017). Efficient Monolithic Perovskite/Perovskite Tandem Solar Cells. Adv. Energy Mater, 7, 1602121

43. Jiang, F., Liu, T., Luo, B., Tong, J., Qin, F., Xiong, S., . . . Zhou, Y. (2016). A two-terminal perovskite/perovskite tandem solar cell. Journal of Materials Chemistry A, 4(4), 1208-1213

44. Zhao, D., Wang, C., Song, Z., Yu, Y., Chen, C., Zhao, X., . . . Yan, Y. (2018). Four-Terminal All-Perovskite Tandem Solar Cells Achieving Power Conversion Efficiencies Exceeding 23%. ACS Energy Letters, 3(2), 305-306

45. Bercx, M., Sarmadian, N., Saniz, R., Partoens, B., & Lamoen, D. (2017). Correction: First-principles analysis of the spectroscopic limited maximum efficiency of photovoltaic absorber layers

ULSAN NATIONAL INSTITUTE OF SCIENCE AND TECHNOLOGY

for CuAu-like chalcogenides and silicon. Physical Chemistry Chemical Physics, 19(8), 6292-6292

46. Stein, J. (2017). PV Performance Modeling Methods and Practices: Results from the 4th PV Performance Modeling Collaborative Workshop

47. Hussain, I., Tran, H. P., Jaksik, J., Moore, J., Islam, N., & Uddin, M. J. (2018). Functional materials, device architecture, and flexibility of perovskite solar cell. Emergent Materials, 1(3-4), 133-154

48. Perovskite progress pushes tandem solar cells closer to market. (2018). C&EN Global Enterprise, 96(24), 16-18

49. Werner, J., Niesen, B., & Ballif, C. (2017). Perovskite/Silicon Tandem Solar Cells: Marriage of Convenience or True Love Story? - An Overview. Advanced Materials Interfaces, 5(1), 1700731

50. Martin A. Green, Anita Ho-Baillie & Henry J. Snaith (2014). The emergence of perovskite solar cells. Nature Photonics 8, 506-514

51. Zhao, Y., & Zhu, K. (2014). CH3NH3Cl-Assisted One-Step Solution Growth of $CH_3NH_3PbI_3$: Structure, Charge-Carrier Dynamics, and Photovoltaic Properties of Perovskite Solar Cells. The Journal of Physical Chemistry C, 118(18), 9412-9418

52. Chueh, C., Liao, C., Zuo, F., Williams, S. T., Liang, P., & Jen, A. K. (2015). The roles of alkyl halide additives in enhancing perovskite solar cell performance. Journal of Materials Chemistry A, 3(17), 9058-9062

53. Xie, Y., Shao, F., Wang, Y., Xu, T., Wang, D., & Huang, F. (2015). Enhanced Performance of Perovskite $CH_3NH_3PbI_3$ Solar Cell by Using CH_3NH_3I as Additive in Sequential Deposition. ACS Applied Materials & Interfaces, 7(23), 12937-12942

54. Zhao, L., Luo, D., Wu, J., Hu, Q., Zhang, W., Chen, K., . . . Gong, Q. (2016). Perovskite Solar Cells: High-Performance Inverted Planar Heterojunction Perovskite Solar Cells Based on Lead Acetate Precursor with Efficiency Exceeding 18% (Adv. Funct. Mater. 20/2016). Advanced Functional Materials, 26(20), 3551

55. Boopathi, K. M., Mohan, R., Huang, T., Budiawan, W., Lin, M., Lee, C., . . . Chu, C. (2016). Synergistic improvements in stability and performance of lead iodide perovskite solar cells incorporating salt additives. Journal of Materials Chemistry A, 4(5), 1591-1597.

56. Bag, S., & Durstock, M. F. (2016). Large Perovskite Grain Growth in Low-Temperature Solution-Processed Planar p-i-n Solar Cells by Sodium Addition. ACS Applied Materials & Interfaces, 8(8),

57. Yang, Y., Zou, X., Pei, Y., Bai, X., Jin, W., & Chen, D. (2017). Effect of doping of NaI monovalent cation halide on the structural, morphological, optical and optoelectronic properties of $MAPbI_3$ perovskite. Journal of Materials Science: Materials in Electronics, 29(1), 205-210.

58. Abdi-Jalebi, M., Dar, M. I., Sadhanala, A., Senanayak, S. P., Franckevičius, M., Arora, N., . . . Friend, R. H. (2016). Impact of Monovalent Cation Halide Additives on the Structural and Optoelectronic Properties of $CH_3NH_3PbI_3$Perovskite. Advanced Energy Materials, 6(10), 1502472

59. Kumar, M. H., Dharani, S., Leong, W. L., Boix, P. P., Prabhakar, R. R., Baikie, T., . . . Mathews, N. (2014). Lead-Free Halide Perovskite Solar Cells with High Photocurrents Realized Through Vacancy Modulation. Advanced Materials, 26(41), 7122-7127

60. Wu, Y., Islam, A., Yang, X., Qin, C., Liu, J., Zhang, K., . . . Han, L. (2014). Retarding the crystallization of PbI_2 for highly reproducible planar-structured perovskite solar cells via sequential deposition. Energy Environ. Sci., 7(9), 2934-2938

ULSAN NATIONAL INSTITUTE OF SCIENCE AND TECHNOLOGY

61. Zhang, T., Yang, M., Zhao, Y., & Zhu, K. (2015). Controllable Sequential Deposition of Planar $CH_3NH_3PbI_3$ Perovskite Films via Adjustable Volume Expansion. Nano Letters, 15(6), 3959-3963

62. Shi, Y., Wang, X., Zhang, H., Li, B., Lu, H., Ma, T., & Hao, C. (2015). Effects of 4-tert-butylpyridine on perovskite formation and performance of solution-processed perovskite solar cells. Journal of Materials Chemistry A, 3(44), 22191-22198

63. Mo, J., Zhang, C., Chang, J., Yang, H., Xi, H., Chen, D., . . . Hao, Y. (2017). Enhanced efficiency of planar perovskite solar cells via a two-step deposition using DMF as an additive to optimize the crystal growth behavior. Journal of Materials Chemistry A, 5(25), 13032-13038

64. Amat, A., Mosconi, E., Ronca, E., Quarti, C., Umari, P., Nazeeruddin, M. K., . . . Angelis, F. D. (2014). Cation-Induced Band-Gap Tuning in Organohalide Perovskites: Interplay of Spin–Orbit Coupling and Octahedra Tilting. Nano Letters, 14(6), 3608-3616

65. www.semicore.com/what-is-sputtering

66. Li, T., Pan, Y., Wang, Z., Xia, Y., Chen, Y., & Huang, W. (2017). Additive engineering for highly efficient organic–inorganic halide perovskite solar cells: Recent advances and perspectives. Journal of Materials Chemistry A, 5(25), 12602-12652

67. Manspeaker, C., Venkatesan, S., Zakhidov, A., & Martirosyan, K. S. (2017). Role of interface in stability of perovskite solar cells. Current Opinion in Chemical Engineering, 15, 1-7

68. Sanehira, E. M., Villers, B. J., Schulz, P., Reese, M. O., Ferrere, S., Zhu, K., . . . Luther, J. M. (2016). Influence of Electrode Interfaces on the Stability of Perovskite Solar Cells: Reduced Degradation Using MoOx/Al for Hole Collection. ACS Energy Letters, 1(1), 38-45

69. Philip Schulz, Jan O. Tiepelt, Jeffrey A. Christians, Igal Levine, Eran Edri,. . . Antoine Kahn (2016), High-Work-Function Molybdenum Oxide Hole Extraction Contacts in 2 Hybrid Organic−Inorganic Perovskite Solar Cell. ACS Appl. Mater. Interfaces. 8, 46, 31491-31499

ULSAN NATIONAL INSTITUTE OF
SCIENCE AND TECHNOLOGY